Reviewed Preprint
v1 • June 26, 2025
Not revised

Reviewed Preprint
v2 • June 17, 2026
Revised by authors

FMRP Regulates Neuronal RNA Granules Containing Stalled Ribosomes, Not Where Ribosomes Stall

Jewel T-Y Li[1], Mehdi Amiri[2,3], Senthilkumar Kailasam[4], Lily Drever[1], Jingyu Sun[5,6], Laura Bohorquez[5,6], Nahum Sonenberg[2,3], Joaquin Ortega[5,6], Wayne S Sossin[1]

[1]Department of Neurology and Neurosurgery, Montreal Neurological Institute, McGill University, Montreal, Canada • [2]Department of Biochemistry, McGill University, Montreal, Canada • [3]Goodman Cancer Institute, McGill University, Montreal, Canada • [4]Canadian Centre for Computational Genomics, McGill University, Montreal, Canada • [5]Department of Anatomy and Cell Biology, McGill University, Montreal, Canada • [6]Centre de Recherche en Biologie Structurale, McGill University, Montreal, Canada

For correspondence: wayne.sossin@mcgill.ca

Competing interests: No competing interests declared

Funding: See page 36

Reviewing editor: Mani Ramaswami, Trinity College Dublin, Ireland

eLife Assessment

Based on several lines of interesting data, the authors conclude that neuronal FMRP, which is associated with stalled ribosomes and mRNP granules, does not determine position on the mRNAs at which ribosomes stall. They instead propose a role in subsequent translational activation of arrested mRNAs. Supported by generally **solid** experimental data, the paper represents a **valuable** contribution to the field. The generality of these conclusions, particularly for neurons of different development stages and for different subtypes of mRNP granules, should become clear with future studies that replicate and extend this work.

https://doi.org/10.7554/eLife.106692.2.sa4

Abstract

Local protein synthesis is a crucial process that maintains local proteostasis in neurons. A large percentage of mRNAs translated in developing neurons are associated with stalled ribosomes. FMRP, the protein lost in Fragile X syndrome, is highly enriched in RNA granules that contain stalled ribosomes. Previous examination of ribosome protected fragments (RPFs) from stalled neuronal ribosomes identified sequences that match those found in mRNAs associated with FMRP, as identified by FMRP cross-linking immunoprecipitation (CLIP) (Anadolu et al, 2023, Journal of Neuroscience doi: 10.1523/JNEUROSCI.1002-22.2023). To investigate whether FMRP recognition of these sequences is important for determining where ribosomes stall on mRNAs, we examined RPFs isolated from P5 mice of both sexes that lack the FMRP protein. We found that the loss of FMRP had no significant effect on the proteins associated with neuronal stalled ribosomes, on ribosome structure, or the stalling sites (locations where RPFs accumulated). However, we observed a small, but significant decrease in the RPF levels from mRNAs previously shown to be associated with FMRP by CLIP in stalled ribosomes. Additionally, the number of neuronal RNA granules containing stalled ribosomes, as assayed by ribopuromycylation, decreased. Unlike neuronal RNA granules in WT neurons, the remaining neuronal RNA granules were resistant to reactivation. These results suggest a role of FMRP in neuronal RNA granules that contain stalled ribosomes, though loss of FMRP does not influence where ribosomes are stalled or the formation of stalled ribosomes.

Introduction

Neurons are structurally unique cells with synapses–sites where neurons connect with each other– often located far from the cell body. For example, hippocampal pyramidal dendrites span an average of 13.5 mm (Ishizuka et al., 1995) while axonal tips can extend up to a meter away from the cell body (Debanne et al., 2011). To maintain and adapt the local proteome in response to local neuronal activity, neurons rely on the ability to produce proteins locally. Indeed, local protein synthesis has been shown to be critical for many aspects of neuronal function including growth cone guidance (Yoon et al., 2009), homeostasis (Holt et al., 2019), aspects of presynaptic firing (Wong et al., 2024) and certain forms of synaptic plasticity (Holt et al., 2019).

Local protein synthesis relies on coordinated mechanisms that couple mRNA transport with translational repression. Two major mechanisms have been proposed to regulate this process in neurons (Kiebler and Bassell, 2006; Sossin and DesGroseillers, 2006). In one mechanism, mRNAs are stalled during initiation and transported within RNA transport particles. In this case, the completion of initiation and onset of elongation depends on the removal of the repression mechanisms and availability of ribosomes, which must be transported separately. In contrast, mRNAs can be transported along with ribosomes when elongation stalls, with stalled ribosomes serving as the transport unit. Both mechanisms are likely to be utilized for neurons. While RNA transport particles appear to facilitate the transport of individual mRNAs (Batish et al., 2012), stalled ribosomes are found within large RNA granules that appear to contain multiple different mRNAs (Langille et al., 2019). The RNA binding protein (RBP) FMRP has been implicated in both types of transport (Richter et al., 2015).

Loss of FMRP causes Fragile X syndrome. In humans, the loss of FMRP results from expansion of a CGG repeat, leading to excessive methylation and transcriptional inhibition. Since CGG expansion is relatively common compared to de novo mutations and the gene is X-linked, Fragile X syndrome is a relatively common neurodevelopmental disorder and is the leading genetic cause of autism (Yu and Berry-Kravis, 2014). FMRP is an RBP and thus plays a role in various aspects of RNA biology. Several of these functions have been implicated in Fragile X syndrome, including FMRP's regulation of miRNA repression, splicing, translation initiation, and translational elongation (Richter et al., 2015; Richter and Zhao, 2021). Another proposed cause of Fragile X syndrome is the loss of protein-protein interactions mediated by FMRP, including the direct regulation of ion channels (Deng and Klyachko, 2021).

A common finding in Fragile X models is that the loss of FMRP increases translation (Huber et al., 2002; Qin et al., 2005). This increase may result from the direct effects of FMRP on translation initiation or elongation, or from the loss of specific FMRP targets, which in turn lead to changes in signal transduction that ultimately increase protein synthesis (Bagni and Zukin, 2019). A major finding regarding how FMRP regulates translation is that, unlike most RBPs, FMRP exhibits strong association with the coding region in cross-linking immunoprecipitation (CLIP) studies, implicating FMRP in stalling elongation (Darnell et al., 2011). Consistent with a role in ribosomal stalling, loss of FMRP caused shifts in polysome profiles of CLIP-identified FMRP targets in Neuro2A translational extracts (Darnell et al., 2011). Additionally, elongation rates are also increased in mouse models of Fragile X, where FMRP is knocked out (Udagawa et al., 2013). While initial studies suggested that FMRP associates non-discriminatively throughout the coding region, more comprehensive bioinformatic analyses have revealed consensus sequences that were enriched in FMRP CLIP data (Ascano et al., 2012; Anderson et al., 2016). FMRP has also been shown to bind to specific motifs such as G quadruplexes and the kissing complex due to the specificity of the RNA-binding domains in the protein (Darnell et al., 2005), but the sequences enriched in FMRP CLIP data do not necessarily contain these motifs (Anderson et al., 2016).

Ribosomes from neuronal RNA granules have been enriched through sedimentation and biochemically and structurally characterized (Krichevsky and Kosik, 2001; Elvira et al., 2006; El Fatimy et al., 2016; Kipper et al., 2022; Anadolu et al., 2023). These ribosomes are stalled in the hybrid state (Kipper et al., 2022; Anadolu et al., 2023) and may possess other modifications

that distinguish them from most ribosomes: For example, unlike most ribosomes, puromycylated peptides do not dissociate from neuronal stalled ribosomes (Anadolu et al., 2024). Additionally, anisomycin competes poorly with puromycin for puromycylation, a property not observed in most ribosomes (Anadolu et al., 2024). Examination of RPFs from these ribosomes have also shown differences from standard preparations. The RPFs are larger than expected and the motifs previously identified in FMRP CLIPs are enriched in the RPF sequences (Anadolu et al., 2023). It is not clear whether the enrichment of FMRP CLIP-associated sequences in RPFs from stalled ribosomes occurs because FMRP determines where ribosomes stall, or whether FMRP associates with stalled ribosomes that were already paused at these specific sequences.

To determine whether FMRP is directly involved in the formation of stalled ribosomes through sequence recognition, we compared RPFs from stalled ribosomes in mice lacking FMRP protein to those in WT mice of the same strain. We also tested whether the larger protected fragments could be reduced in size by higher nuclease treatment. Our findings show that stronger nuclease treatment does reduce the size of RPFs to a normal size. Despite its enrichment in RNA granules containing stalled ribosomes, FMRP does not appear to be important for the formation of stalled ribosomes since the loss of FMRP did not affect the association of other proteins with stalled ribosomes, the state of the stalled ribosomes, and, most importantly, where the ribosomes stall. However, using ribopuromycylation (RPM) to detect RNA granules containing stalled ribosomes (Graber et al., 2013), we found that the loss of FMRP decreased the number of RPM puncta. Thus, FMRP may contribute to stabilizing RNA granules.

Results

Comparing RNA Binding Protein Enrichment in WT and FMR1- RNA Granules

Stalled ribosomes are found in neuronal RNA Granules (Graber et al., 2013). Previous studies have demonstrated that in brain homogenates, a substantial number of ribosomes sediment in sucrose gradients used to separate monosomes from polysomes, and these have been suggested to be the ribosomes in neuronal RNA granules (Krichevsky and Kosik, 2001; Aschrafi et al., 2005; Elvira et al., 2006). This sedimentation was further optimized to separate the ribosomes found in the pellet from heavy polysomes (Fig. 1A) (El Fatimy et al., 2016; Anadolu et al., 2023). To determine whether the pellet from C57BL-6 mice is comparable to the pellet from rat brains in a previous study (Anadolu et al., 2023), we examined the protein distribution across all collected fractions from each species' brain homogenate using Coomassie blue staining. The protein distribution was similar between rat brain and WT mouse brain with considerable amounts of proteins in both WT-mouse pellet and rat pellet (Fig 1B).

We compared fractionation between WT and FMR1 knockout mice (FMR1-). FMR1-mice is the most common model for studying FMRP's function (Richter and Zhao, 2021). There was no change in the distribution of UV absorbance in the fractions in the presence or absence of FMRP (Fig. 1C). We specifically compared fractions 5 and 6 from the gradient to the pellet to be consistent with previous studies (El Fatimy et al., 2016; Anadolu et al., 2023) comparing ribosomes in clusters that pellet and ones that do not. EM of fraction 5/6 and the pellet showed an abundance of ribosome clusters in both fractions in the presence or absence of FMRP (Fig. 1D). We examined the distribution of proteins in three fractions: the starting material after the first spin to remove non-soluble material, fraction 5/6, and the pellet, similar to the fractions examined in earlier studies (El Fatimy et al., 2016; Anadolu et al., 2023). We confirmed previous results from rat (Anadolu et al., 2023) that in WT mice FMRP (1.9 +/- 0.54 S.D, n=4, $p<0.05$ one sample T-test against 1) and UPF1 (1.5 +/- 0.57, S.D, n=8, $p<0.05$, one sample T-test against 1) were enriched in the pellet fraction vs fraction 5/6. As well, both Staufen 2 bands quantified (upper; 59 kDa and lower; 52 kDa) were enriched in the pellet fraction vs fraction 5/6 (59 kDa; 3.9 +/- 1.8, S.D, n=8, $p<0.01$, one sample t-test against 1; 52 kDa; 3.4 +/- 1.8, S.D, n=8, $p<0.01$, one sample t-test against 1).

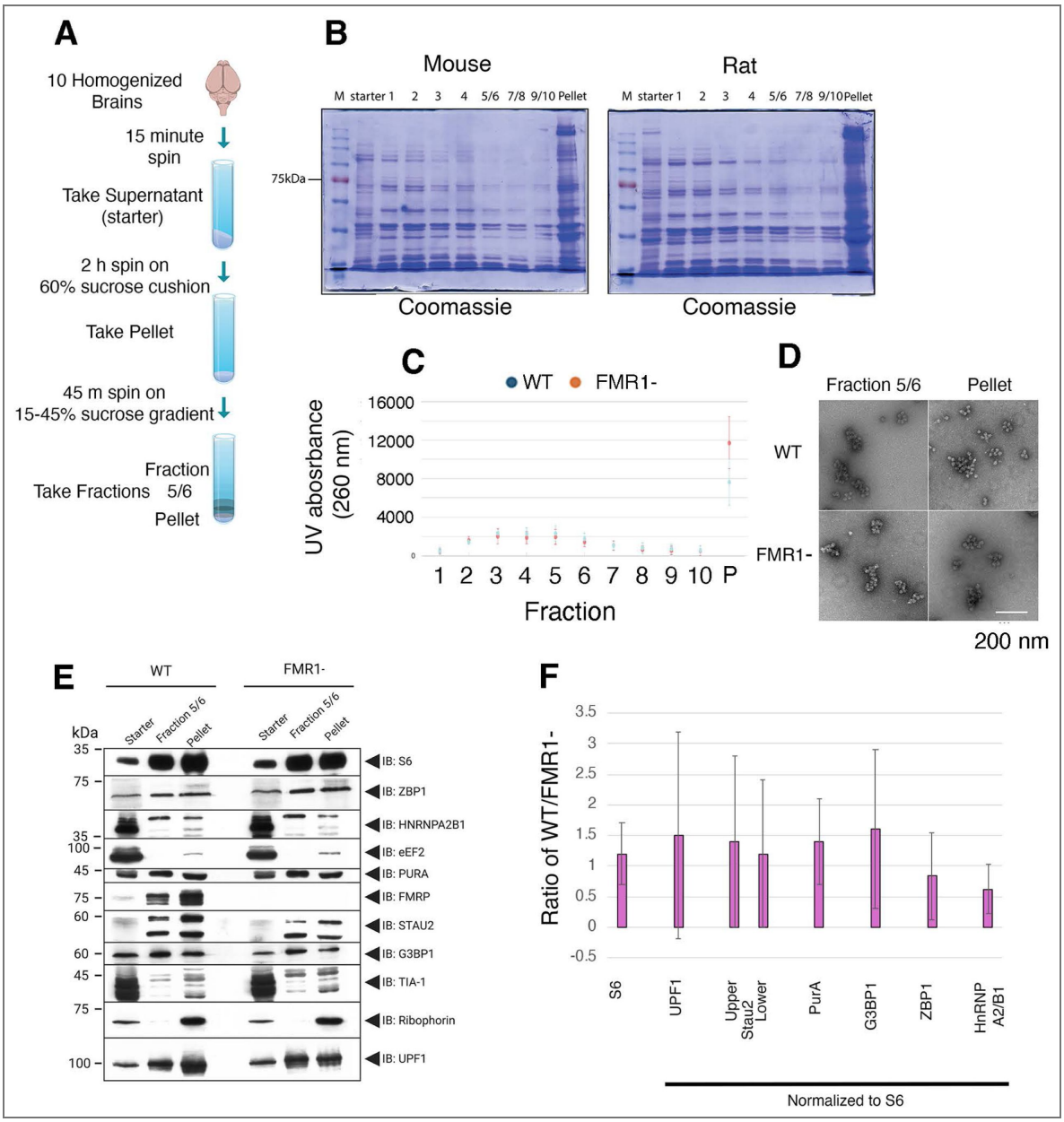

Figure 1. Characterization of Sucrose Gradient Sedimentation.

A) A summary of the protocol for isolating the pellet and fraction 5/6 from mouse and rat whole brain homogenate using sucrose gradient fractionation. B) SDS-page stained with Coomassie brilliant blue showing the distribution of proteins from each fraction of the sucrose gradient from mouse and rat brains. Equal volumes of resuspended ethanol precipitates (fractions 1-10) and resuspended pellet were used. C) Average UV absorbance from fractions 1-10 and pellet from WT (Red) and FMR1- (blue) preparations (Error bars are S.D., N=3). D) Representative electron microscopy of WT and FMR1- ribosome clusters from fraction 5/6 and pellet. Scale bar is 200 nm). E) Representative immunoblots of fractions (as defined in A) for WT and FMR1- mice. For each blot, 1/100th of the Starter, 1/10th of Fraction 5/6 and 1/20th of the pellet fraction were loaded. F) Quantification of differences in enrichment between WT and FMR1-. Levels of proteins were determined from scans of immunoblots (see methods). Enrichment is defined by the ratio of level of protein (see Methods) between Fraction 5/6 and Pellet. For S6, the ratio of WT enrichment to FMR1- enrichment was calculated for each blot and the average calculated (N=8). For all the other RBPs, the WT and FMR1- enrichment were normalized to the S6 enrichment for that preparation and the normalized values were used to calculate the difference in enrichment between WT and FMR1- (UPF1, n=8, Stau2, n=8, PurA, n=3, G3BP1 (n=3), ZBP1 (N=3), hnRNPA2/B1 (N=3). Error bars are S.D. A one sample T-test against 1 was used to test significance with Bonferroni correction for multiple tests. No value reached $p < 0.05$.

We next compared the level of ribosomal protein S6 as a marker of ribosomes between WT and FMR1- mice. If FMRP was critical for the formation of the clustered ribosomes in the pellet, there should be fewer ribosomes in the pellet compared to fraction 5/6 in the absence of FMRP. However, we observed no significant difference in the ratio of S6 between these two fractions in the presence or absence of FMRP (Fig. 1E, quantified in Fig. 1F). We also compared the fractionation of proteins implicated in RNA transport in neurons between WT and FMR1-mice: UPF1 (Graber et al, 2017); Stau2 (Tang et al., 2001; Heraud-Farlow and Kiebler, 2014; Graber et al., 2017); Zip code binding protein 1 (ZBP1) (Huttelmaier et al., 2005), Pur alpha (Kanai et al., 2004), G3BP1 (Anadolu and Sossin, 2020) and hnRNP A2/B1(Gao et al., 2008; Lo et al., 2025). No significant differences in fractionation for any of these proteins were observed in the presence or absence of FMRP (Fig. 1E, quantified in Fig. 1F). TIA-1, a protein present in stress granules, but not neuronal RNA granules (Anadolu and Sossin, 2020; Sun et al., 2025) was mainly in the starter fraction. We examined eEF2 and confirmed previous results (Anadolu et al., 2023) that there was little eEF2 in either fraction 5/6 or the pellet under these conditions (Fig. 1E). We also examined the rough ER marker ribophorin. While previous results showed that secretory mRNAs showed low abundance in the pellet compared to most mRNAs, the secretory mRNAs were enriched in the pellet compared to fraction 5/6 (Anadolu et al., 2023). To determine if this is due to increased presence of rough ER in the pellet fraction vs fraction 5/6, we examined distribution of the rough ER marker ribophorin. We observe ribophorin protein in the pellet, but not in fraction 5/6 and this was not affected by FMRP (Fig. 1E).

Loss of FMRP Does not Alter Anisomycin Puromycin Competition

Previous cryo-EM studies of ribosomes isolated from dense ribosome clusters showed that most of these ribosomes are in the hybrid A/P and P/E configuration (Kipper et al., 2022; Anadolu et al., 2023). Puromycin and anisomycin are both translational inhibitors that bind to the A site of the ribosomes (Hansen et al., 2003; Garreau de Loubresse et al., 2014). Due to their overlapping binding sites, anisomycin inhibits puromycin from binding to the ribosomes when both are present. However, we previously showed that puromycylation of neuronal ribosomes in cell culture and puromycylation of ribosomes in the pellet from rats are resistant to anisomycin inhibition (Anadolu et al., 2024). This suggested that the binding site for these translational inhibitors is altered in the neuronal stalled ribosome, either due to the enrichment of the hybrid state or due to other differences in these ribosomes.

We performed these experiments on the ribosomes that were sedimented through the sucrose gradient (Fig 2A). We first validated that puromycylation in non-neuronal ribosomes, in this case- rat liver ribosomes, were not resistant to anisomycin. Indeed, we saw a total inhibition of puromycylation by anisomycin in sedimented rat liver ribosomes (Fig 2B) much like the effect previously seen on HEK cell culture (Anadolu et al., 2024). This indicated that neither homogenization in our buffer nor high centrifugation is sufficient to confer puromycin's resistance to anisomycin and further confirmed the neuronal specificity of this ribosomal state. If FMRP was important for generating the state of the ribosome required for anisomycin-resistant puromycylation, we should observe less resistance to anisomycin in FMR1- mice. We found that resistance of puromycylation to anisomycin was not different in ribosomes from the pellet of WT and FMR1- mice (Fig. 2B, quantified in Fig. 2C). Thus, FMRP does not seem to be important for the formation of this state of the ribosome.

Effects of Digestion on RPF Size

To explore if the stalling sites of the ribosomes are altered by the loss of FMRP, we examined RPFs (Fig. 3A). RPFs generated from the rat pellet were generally above 35nt (Anadolu et al., 2023), while RPFs have a canonical size between 28nt and 32nt (Ingolia, 2014). It was unclear whether the extension at the 3' end from the RPF generated from the pelleted rat ribosomes was due to an extended conformation of the ribosome to protect a larger fragment or due to altered nuclease resistance in this region (Anadolu et al., 2023). Thus, we investigated whether this extended region could be cleaved off with more effective nuclease treatment. To determine whether the

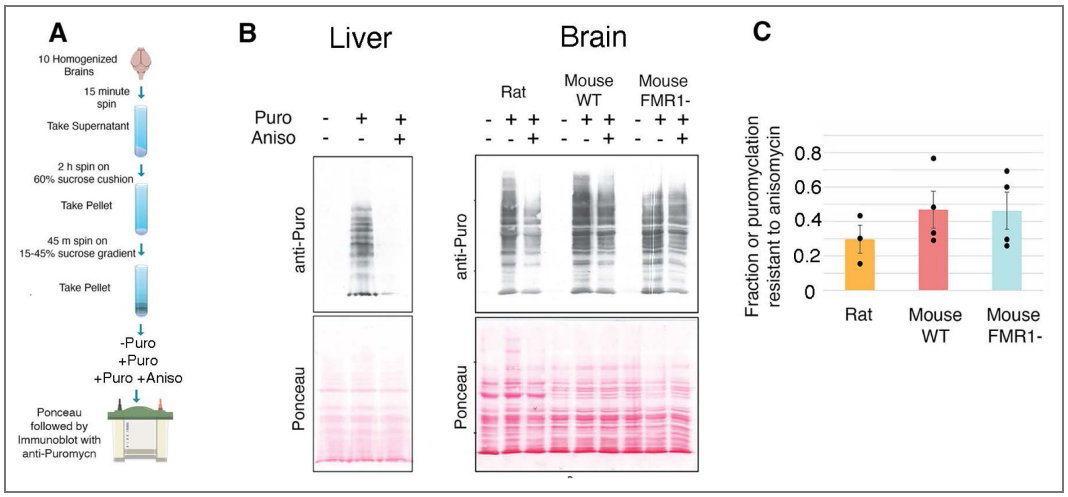

Figure 2. Loss of FMR1 does not affect anisomycin-puromycin competition.

A) A summary of protocol for isolating the pellet and treating with puromycin. B) Representative immunoblot stained with antibodies to puromycin (anti-puro) (Top) to showcase the inhibition of puromycylation (100 uM) by anisomycin (100 uM) in liver polyribosomes (left) or comparing the pellet from Rat, Mouse WT and Mouse FMR1- (Right). Bottom: Corresponding membrane stained with Ponceau before immunoblotting. The liver experiment was replicated twice with similar results. C) Quantification of the amount of puromycylation resistant to anisomycin (puro +aniso/ puro) in Rat (N = 3), WT mouse (N = 4), FMR1- (N = 4). All groups are insignificant from each other (one way ANOVA, $p > 0.05$).

extending nucleotides could by removed by increasing nuclease efficiency, we digested at room temperature rather than 4°C, and in addition, the concentration of RNAse was adjusted to the sample RNA concentration (see Methods).

We replicated the increased size of RPFs in mice using the low nuclease protocol. However, RPFs generated by the new nuclease treatment decreased the RPFs to around 29-30 nt (Fig 3B). While there was still a portion of RPFs that stayed around 35 nt (Fig 3B), the majority of these RPFs are from noncoding mRNAs (Extended Data Table S3-1). The new nuclease treatment also showed a higher percentage of RPFs in the coding region (CDS) (Fig. 3C), no extension on the 3' end (Fig. 3D) and a higher periodicity (Fig. 3E). These results were consistent across all libraries (Fig. S3-1, S3-2, S3-3). For all analysis below, we use only the RPFs from the new (standard) nuclease treatment.

Higher $MgCl_2$ Concentrations did not Affect Ribosomal Structure

An additional change from the previous protocol was in the concentration of $MgCl_2$. Most ribosome isolation protocols use 10 mM $MgCl_2$, but the previous protocol had a more physiological concentration of 2.5 mM $MgCl_2$. Higher levels of $MgCl_2$ in most protocols that purify ribosomes are presumably due to the finding that bacterial ribosomes dissociate in lower concentrations of $MgCl_2$, but this has not been observed in eukaryotic ribosomes. A cryo-electron microscopy (cryo-EM) characterization of RNase I-treated pellet fraction under this low magnesium concentration (Anadolu et al., 2023) found that 85% of the ribosomes contained in the pellet exhibited tRNA molecules in hybrid A/P and P/E state. The remaining 15% of the ribosome population in this sample contained a tRNA in the P/P state. To test whether increasing the magnesium concentration had any effect on the percentage of ribosomes in hybrid A/P and P/E state, we repeated the cryo-EM and image classification analysis (Fig. S4-1) after the purification was performed in a buffer containing 20mM Tris-HCl, pH 7.4; 150 mM NaCl; 10 mM $MgCl_2$. We found that high $MgCl_2$ did not impact the percentages of hybrid A/P and P/E state (83%) and P/P (17%) state ribosomes (Fig. 4A). The cryo-EM maps for the hybrid and P/P state ribosomes were refined to 2.7 Å and 3.2 Å, respectively (Fig. S4-2 and Table S4-1).

Characterization of the RPFs of mRNAs in WT and FMR1- Pellet through DEG, GO and GSEA Analysis

To analyze the mRNAs in the WT and FMR1- pellet, we mapped the data from RNA-seq and the RPFs to their corresponding mRNAs (Fig. 5A), similar to our previous analysis of RPFs from rat (Anadolu et al., 2023). PCA analysis shows that the variation between samples was similar to the difference between WT and FMR1- and that there was a large difference between the sequences in the RPFs and RNA-seq (Fig. S5-1). To compare the samples across different biological preparations, we calculated the reads per kilobase per million mapped reads (RPKM), which normalized the mRNA count against the total mapped count and gene length (Extended Data Table 5-1). We use the term abundance for the RPKM of RPFs found in the pellet fraction. The number of RPFs normalized against total mRNA obtained from whole brain homogenate with RNA-seq, often termed translational efficiency, was also calculated as the log(fold change) log (FC) (Extended Data Table 5-2). We refer to this measure as ribosome occupancy (Anadolu et al., 2023) since the subject of this study is stalled ribosomes and thus the number of ribosomes/mRNA is related not only to translational efficiency, but also to stalling. Lastly, we normalized the RPKM of the RPFs in the pellet against the RPKM of RPFs in fraction 5/6 as log (FC) to determine the extent to which mRNAs are selectively found in the pellet fraction (Extended Data Table 5-2). We call this value enrichment (Anadolu et al., 2023) to reflect enrichment in the pellet fraction.

We used DEG analysis to determine differences in RPFs beetween WT and FMR1-. Only a few differences were observed between RKPM values in WT and FMR1- RNA-seq samples (Extended Data Table 5-2). Similarly, there were very few differences using DEG analysis for abundance, occupancy or enrichment between WT and FMR1- (Extended Data Table 5-2). GO analysis of the top 500 abundant or occupied mRNAs gave similar results in WT and FMR1-mice and these results

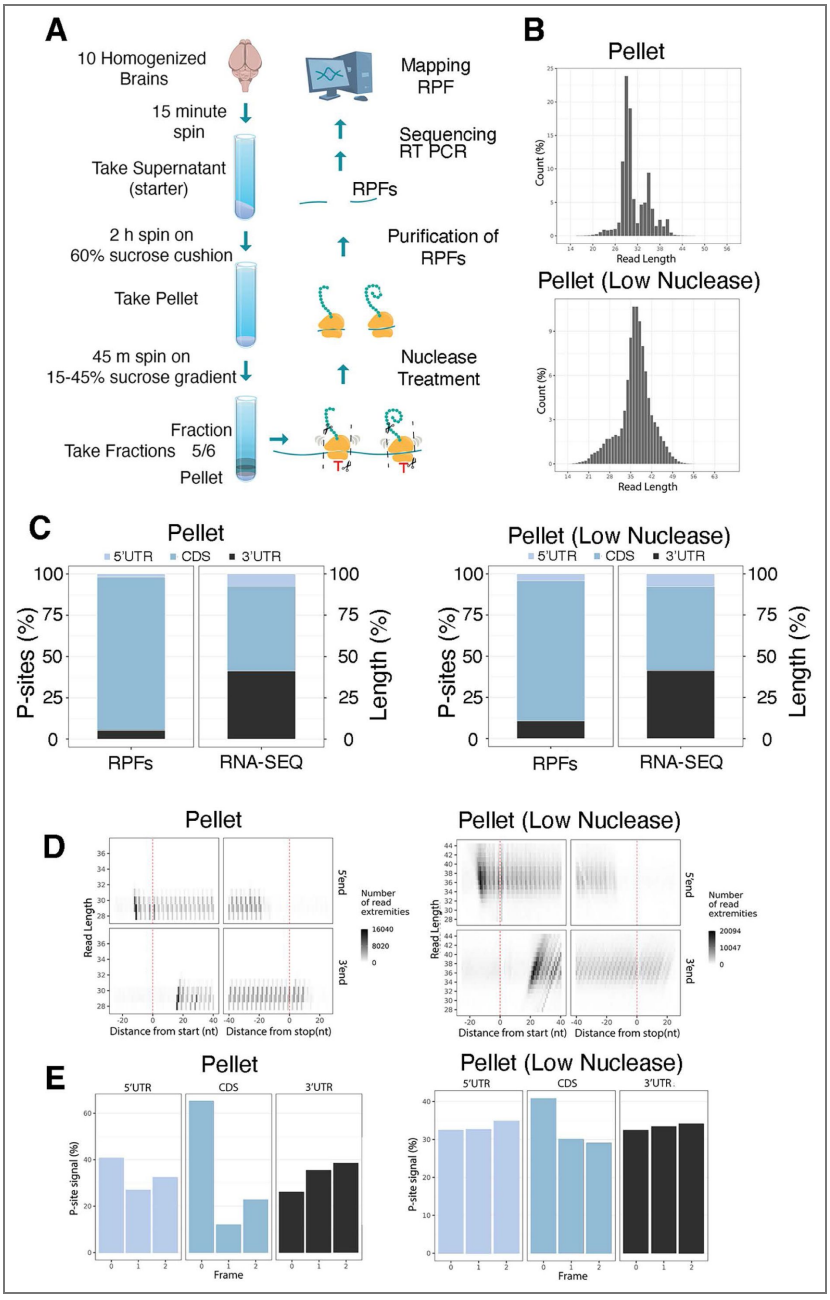

Figure 3. Higher Nuclease Reduces Size of RPFs in WT Pellet.

A) A summary of the protocol for the RPF procedure. B) Size distribution of normalized footprint reads from the WT Pellet fraction under standard or low nuclease treatment. C) Representative image for read coverage for WT Pellet fraction either with standard or low nuclease treatment) UTR, untranslated region; CDS, coding sequence for both RPFs and RNA-seq libraries. D) Representative image for the number of read extremities (shading) for each read length (Y-axis) based on the distance from start(left) to stop(right) with the 5′ end (top) and 3′ end (bottom) for the WT pellet fraction with either standard or low nuclease treatment. E) Representative image for the periodicity statistics for RPFs in different regions of the mRNA for standard or low nuclease treatment. Although the representative images above included only one replicate, similar results were observed across all three replicates.

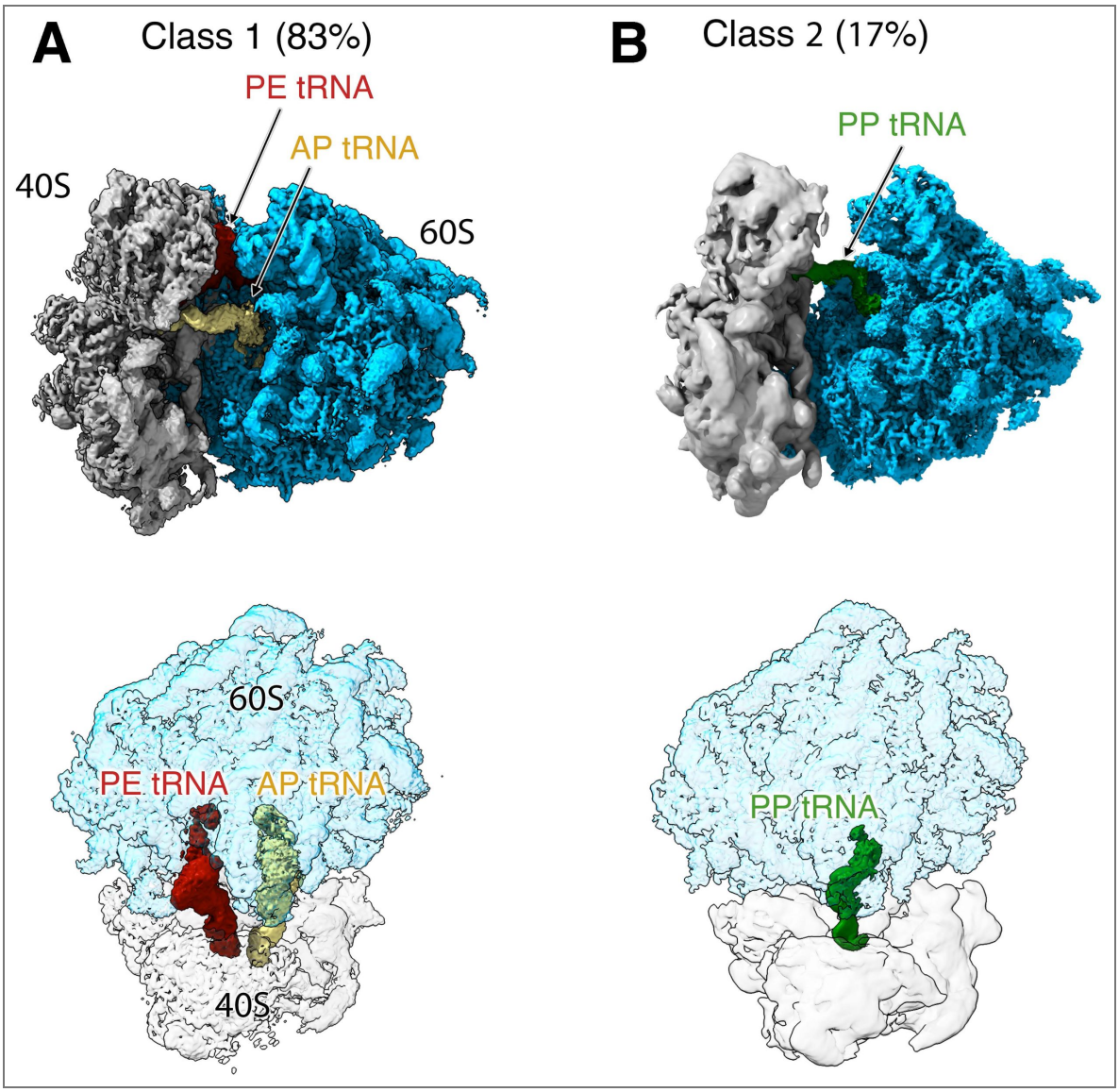

Figure 4. **High Magnesium Buffer does not Affect Ribosome structure**

Composite cryo-EM maps of class 1 (A) and class 2 (B) 80S ribosomes found in the pellet after purification in high magnesium buffer and RNase I treatment. The top panels show a side view of the two classes of ribosome particles contained in the sample. The bottom panels show top views of the same cryo-EM maps. The 40S and 60S subunits are shown as transparent densities to facilitate visualization of the positions of the tRNA molecules in each class.

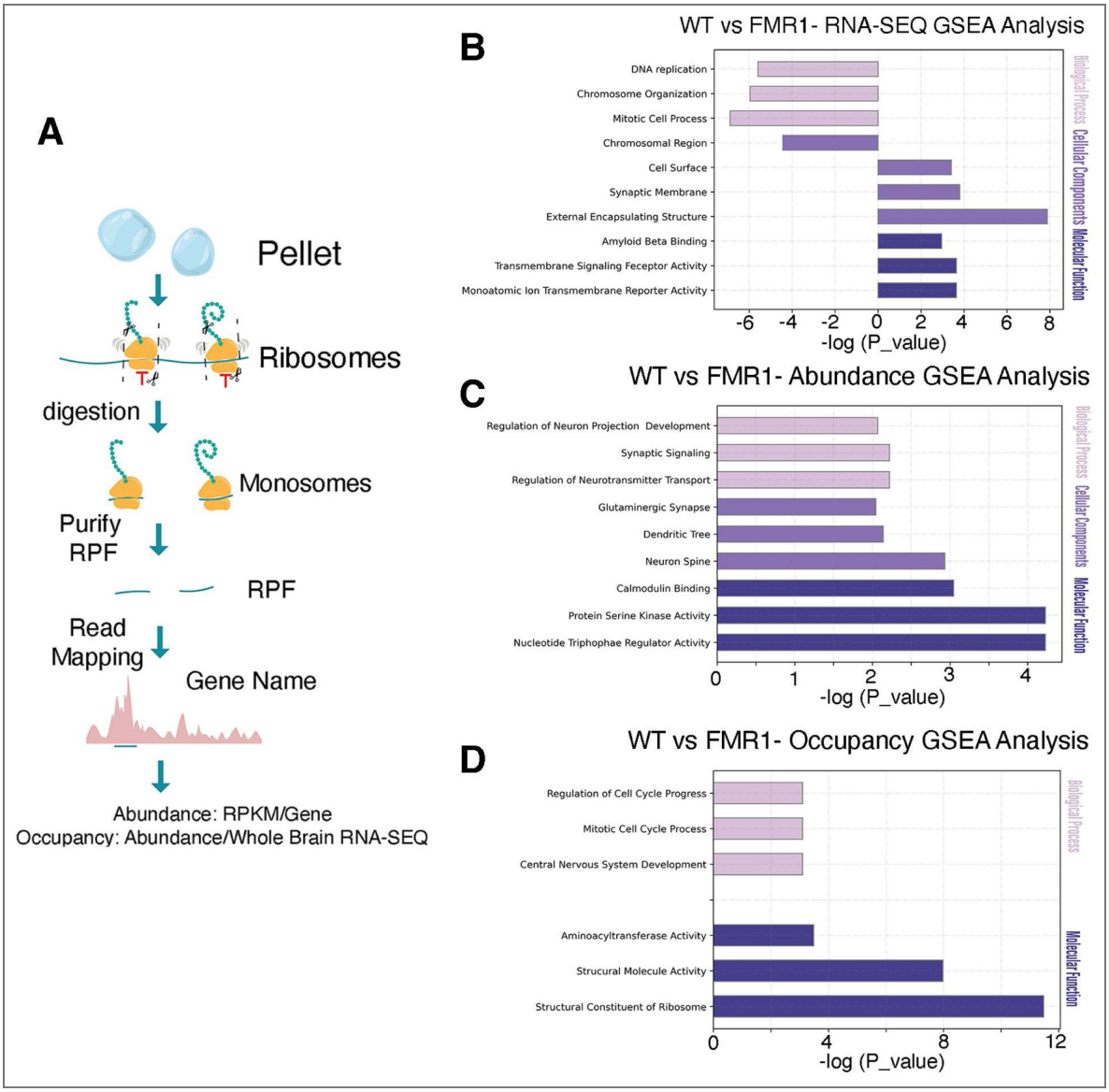

Figure 5. GSEA analysis WT and FMR1- RNA-seq and RPFs from pellet fraction

A) Description of RPF isolation and mapping. Results of Selected GSEA sets significantly affected by the loss of FMRP from analysis of B) RNA-seq, C) Abundance and D) Occupancy. Increases in FMR1- vs WT are to the left and decreases to the right.

(increased abundance of cytoskeletal mRNAs and increased occupancy of mRNAs encoding proteins involved in RNA processing) were similar to previous results in rats (Figure S5-2; Extended Data Table 5-3) (Anadolu et al., 2023).

As another way to compare mRNAs between the two groups we used gene set enrichment analysis (GSEA) comparing WT and FMR1- samples (Fig. 5A, Extended Data Table 5-4). In the RNA-seq analysis, this revealed several gene sets whose levels increased or decreased upon loss of FMRP (Fig. 5B, Extended DataTable 5-4). This analysis revealed a decrease of the abundance of gene sets in FMR1- samples (Fig. 5C). GSEA sets identified as decreased in abundance in the pellet included postsynapse, neuron, spine, dendritic tree and protein kinases (Fig. 5C, Extended Data Table 5-4). There were also some gene sets that had decreased occupancy including cell component structural component of the ribosome, and nervous system development. There were no GSEA sets identified as changed in enrichment (Extended Data Table 5-4). We determined whether the modified mRNAs identified in the GSEA analysis were enriched for FMRP targets as defined by RNA CLIP studies (Darnell et al, 2011). Approximately 4% of the total mRNAs are FMRP targets and approximately this percentage of the gene sets identified in RNA-seq or measuring occupancy matched this expected number (Extended Data Table 5-4). In contrast, the gene sets decreased in abundance by the loss of FMRP had about 30% FMRP target mRNAs in the mRNAs changed. (Extended Data Table 5-4). This suggested that there may be a decrease in the levels of FMRP target mRNAs in the pellet.

Comparison of the mRNAs in the WT and FMR1- to Selected Datasets

Previously, we showed that specific mRNA subsets are enriched in the pellet (Anadolu et al., 2023). We first examined the the abundant mRNAs associated with ribosomes resistant to ribosome runoff (Shah et al., 2020) (Extended Data Table 6-1). Similar to previous experiments with rats (Anadolu et al., 2023), the mRNAs resistant to run off were significantly abundant, occupied and enriched in both WT and FMR1- pellet RPFs (Fig 6). Next, we investigated FMRP associated mRNAs (FMRP targets) through assessing mRNAs identified by cross-linking FMRP with mRNA (Darnell et al., 2011; Maurin et al., 2018) (Extended Data Table 6-1). We found that FMRP targets were highly abundant and enriched in the WT and FMR1-pellet (Fig 6A, Fig 6C, Fig 6E), but the increase in occupancy was less than that observed for the mRNAs resistant to run-off. The increase in occupancy compared to total mRNAs was even less in the FMR1-samples.

To better understand this change after the loss of FMRP, we next examined the specific effect of the loss of FMRP on these subsets of mRNA by calculating the fold change in abundance, occupancy, and enrichment of these specific mRNAs between WT and FMR1-pellets compared to changes in all mRNAs (Fig. 7; (Extended Data Table 7-1). This revealed a significant decrease in the abundance, occupancy and enrichment of the FMRP targets. Strikingly, while there was also a decrease in the abundance and enrichment of mRNAs resistant to ribosome runoff, their occupancy did not change after the loss of FMRP. It should be noted that the decreases of FMRP targets in the FMR1- pellet were small (Fig. 7) and only significant when looked at in the whole subset. Individual mRNAs in this group were not found to be significantly different in the DEG analysis (Extended Data Table 5-2).

The difference between the mRNAs resistant to run off and the FMRP targets in these analyses is surprising as over 60% of the mRNAs resistant to run off are also FMRP targets. We examined the mRNAs resistant to run-off separately based on whether or not they were FMRP targets (Extended Data Tables 6-1, 7-1 and Fig S7-1). This revealed that the lack of an effect of FMRP loss in this group was due to the absence of an effect on mRNAs resistant to run-off that were not FMRP targets (Fig. S7-1). Even more striking was the comparison between the occupancy of FMRP targets that were or were not also mRNAs resistant to run-off. FMRP targets that were not also resistant to run-off (85% of this group) showed no increase in occupancy (Fig S7-1). Thus, FMRP targets showed increased abundance and enrichment compared to total mRNAs and decreases in all features in the absence of FMRP (Fig S7-1). In contrast, mRNAs resistant to run-off showed

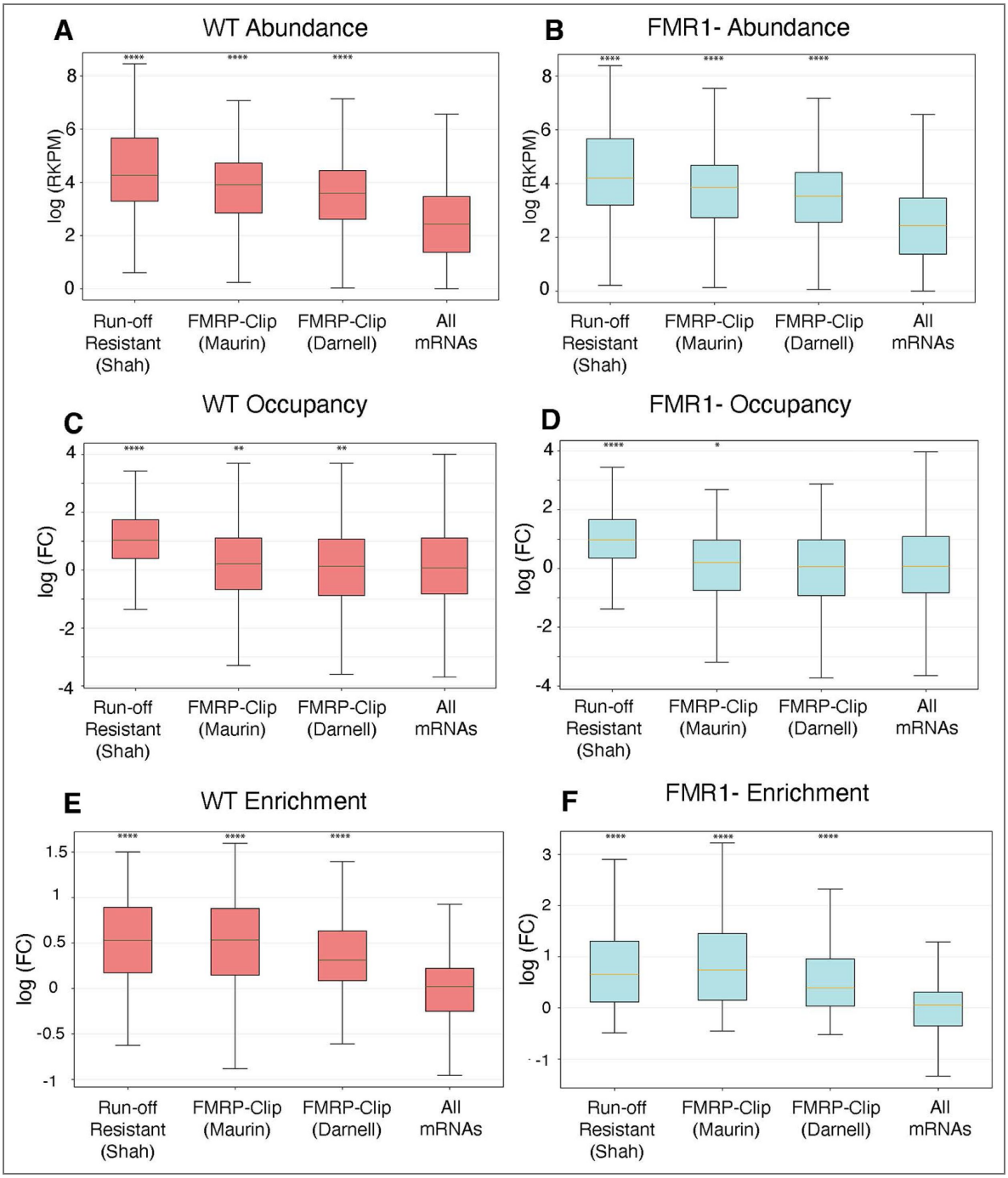

Figure 6. Comparison of Putative Stalled mRNAs vs Total mRNAs in RPFs from the Pellet of WT and FMR1- mice.

Comparison of mRNAs associated with ribosome resistant to initiation inhibitor mediated run-off (Shah et al., 2020) and FMRP-CLIPped mRNAs (Maurin et al., 2018; Darnell et al., 2011) to all other mRNAs. A) WT Pellet abundance, B) FMR1- Pellet abundance, C) WT Pellet Occupancy, D) FMR1-Pellet Occupancy, E) WT Enrichment, and F) FMR1- Enrichment. As the N of the All mRNAs (13079) were much larger than for the selected groups: Shah (185), Maurin (264), Darnell (757) (Extended Data Table S6-1) a random set from the total RNA group that matched the number in the selected group was generated for a two-tailed Welch's T-test with Bonferroni correction for multiple T-tests. The median P value from 10 random sets was used (Extended Data Table S6-1). (****, p<0.0001, ***, p<0.001, **, p<0.01, *, p<0.05).

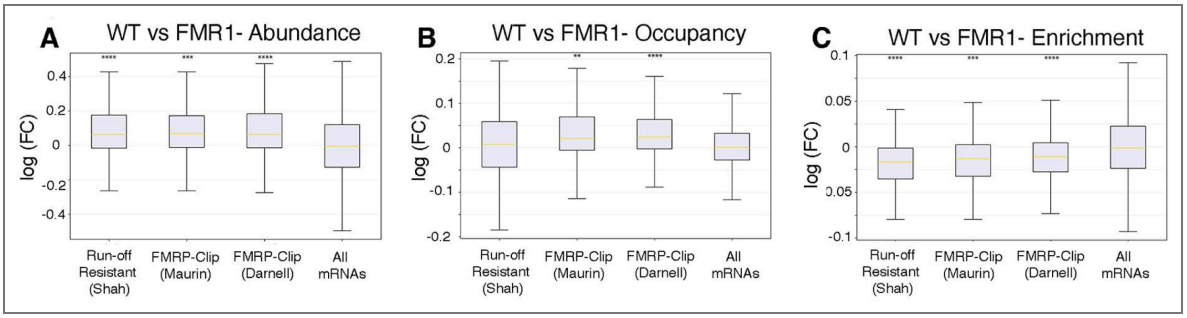

Figure 7. Comparison of Putative Stalled mRNAs between WT and FMR1- mice.

Comparison of mRNAs associated with ribosome resistance of initiation inhibitor run-off (Shah et al., 2020) and FMRP-CLIPped mRNAs (Maurin et al., 2018; Darnell et al., 2011) to all other mRNAs. The fold change between WT and FMR1- was calculated using DEG (see Methods). These fold changes were then compared between the selected groups and All mRNAs for A) Pellet abundance, B) Pellet occupancy, C) Pellet enrichment. As the N of the All mRNAs (13079) were much larger than for the selected groups: Shah (185), Maurin (264), Darnell (757) (Extended Data Table S7-1) a random set from the total RNA group that matched the number in the selected group was generated for a two-tailed Welch's T-test with Bonferroni correction for multiple T-tests. The median P value from 10 random sets was used (Extended Data Table S7-1). (****, p<0.0001, ***, p<0.001, **, p<0.01, *, p<0.05).

higher occupancy than total mRNAs or FMRP targets and showed decreased abundance and enrichment in the absence of FMRP, but their occupancy was not affected by the loss of FMRP (Extended Data Tables 6-1, 7-1 and Fig. S7-1).

Peak Analysis of RPFs in the WT and FMR1- Pellet

The distribution of RPFs in stalled ribosomes is dominated by peaks, presumably representing stalling sites. Our previous result showed that RPFs in the peaks from the pellet were enriched with FMRP related mRNA motifs (Anadolu et al., 2023). Thus, to inquire if the loss of FMRP altered the location of stalled ribosomes, peaks were identified in each of the six pellet preparations (3 WT and 3 FMR1-) (Fig. 8A)

We identified 615 peaks that were present in all six samples. In contrast, there were many fewer peaks solely present in WT or solely FMR1-: 181 peaks for WT and 125 peaks for FMR1-(Extended Data Table 8-1; Fig. 8B). Thus, most peaks were present in both the WT and FMR1-pellets. In general, the distribution of RPF peaks is quite similar in different biological preparations, as exemplified by the Tubb2b mRNAs (Fig. 8C), a cytoskeletal mRNA that shows high ribosomal occupancy in our samples and that was also examined in the previous manuscript (Anadolu et al., 2023).

Moreover, similar to our previous results, the majority of peaks (74-80%) contain a FMRP related motif, and this was not different in the peaks that were enriched in all the samples and the peaks that were only identified in the WT (i.e not seen in FMR1- mice) or only in FMR1-mice (i.e. not seen in WT mice) (Figure 8B). Previously, we found that these peaks were enriched in negatively charged amino acids, glutamic acid and aspartic acid. This was also true for the peaks here, regardless of whether they were present or absent in the FMR1- mice (Fig. 8B).

Loss of FMRP Decreases the Number of RNA granules containing Stalled Ribosomes

Since FMRP did not appear to affect the location on mRNAs where the ribosomes were stalled, we next examined the number and size of neuronal RNA granules containing stalled ribosomes in WT and FMR1- hippocampal cultures (Fig. 9A). FMRP is localized to neuronal RNA granules in hippocampal neuronal cultures (Graber et al., 2013; El Fatimy et al., 2016). We examine neuronal RNA granules containing stalled ribosomes in hippocampal neurons using a technique called ribopuromycylation (RPM)(David et al., 2013). The ribosomes covalently link puromycin to nascent peptide chains on ribosomes in a process called puromycylation and these ribosomes are then identified with an antibody to puromycin. Stalled ribosomes are identified by incubating with an initiation inhibitor, in this case homoharringtonine (HHT), to run off translating ribosomes before puromycylation. While in non-neuronal cells, puromycylated peptides leave the ribosome (Enam et al., 2020; Hobson et al., 2020), puromycylated nascent chains are retained on neuronal stalled ribosomes, perhaps due to a peptide-mediated ribosomal stall (Anadolu et al., 2024). Thus, RPM remains appropriate for localizing stalled ribosomes in neurons.

We examined RPM puncta (Fig. 9A) in neurites >50 microns from the cell soma as there was too much RPM signal proximal to this to distinguish puncta clearly. We found that the number of RPM puncta were significantly decreased in hippocampal cultures from mice lackingFMRP (Fig, 9B quantified in Fig. 9C). There were no differences in the average size of the remaining puncta (Fig. 9B, quantified in Fig. 9D) and the RPM puncta were equally resistant to both run-off with HHT and competition with anisomycin (Fig. S9-1) consistent with these puncta representing large collections of neuronal stalled ribosomes. Previously we showed that dihydroxyphenylglycine (DHPG), an agonist of metabotropic glutamate receptors (mGluRs) can reduce the number of RPM puncta in these cultures (Graber et al., 2013). The decrease of these RPM puncta is coincident with the reactivation of translation from stalled ribosomes by DHPG at this time point (DIV8-10) (Graber et al., 2013; Graber et al., 2017). Moreover, long-term depression (LTD) induced by DHPG is blocked by elongation inhibitors, but not initiation inhibitors, consistent with DHPG activating protein synthesis required for mGluR-LTD by

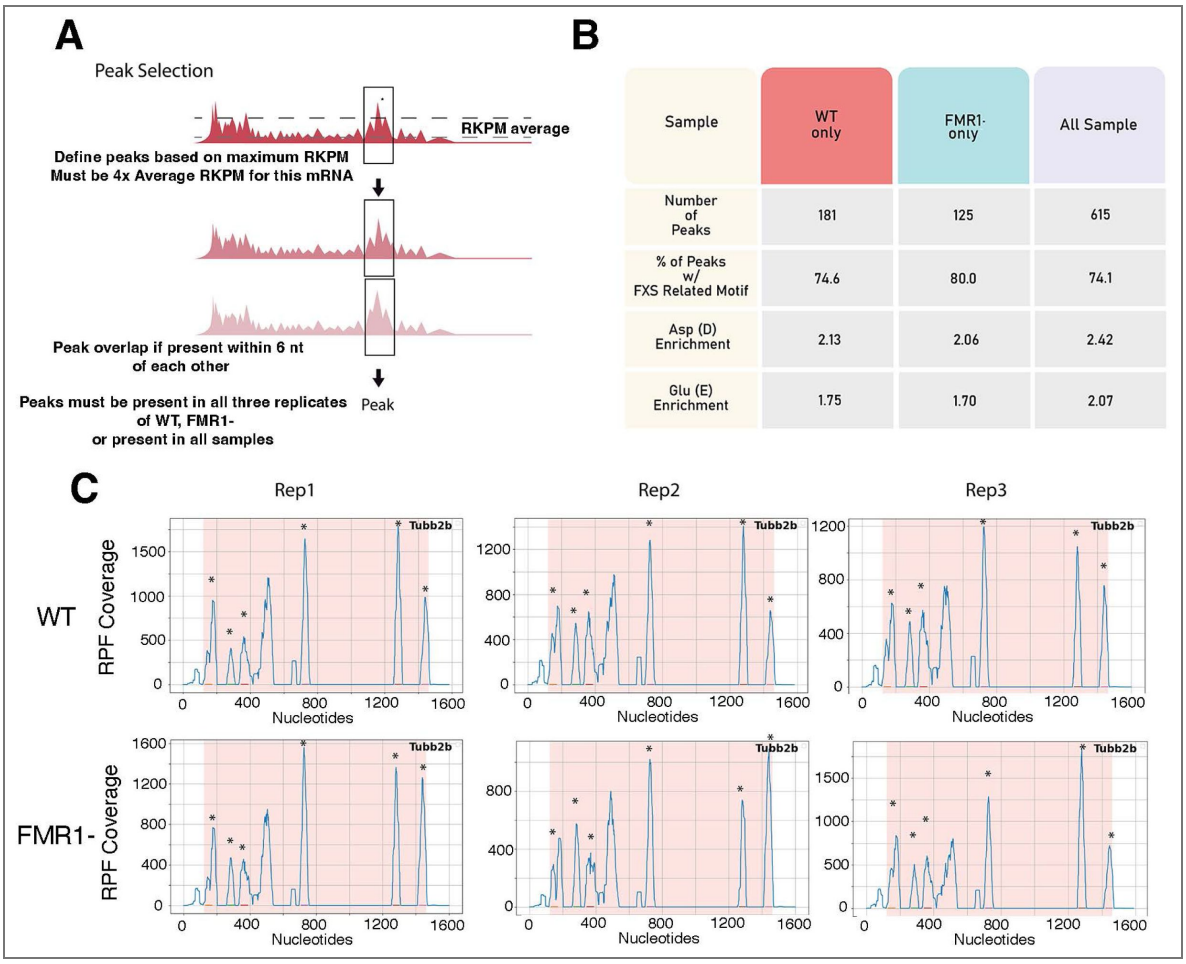

Figure 8. Comparison of RPF peaks in the pellet of WT and FMR1- mice.

A) Representation of how peaks of RPFs are selected. B) Table of the number of peaks between replicates of WT Pellet (N = 3), FMR1- Pellet (N = 3) and combined (N = 6), the percentage of peaks with FXS related motif and the enrichment of Aspartate (Asp) and Glutamate (Glu) in the peaks compared to non-peaks (Extended Table S8-2). C) RPF coverage of Tubb2b for the three replicates of WT and FMR1-. Shaded region is the open reading frame. Asterisks indicate consensus peaks (seen in all six samples with peaks within 6 bp).

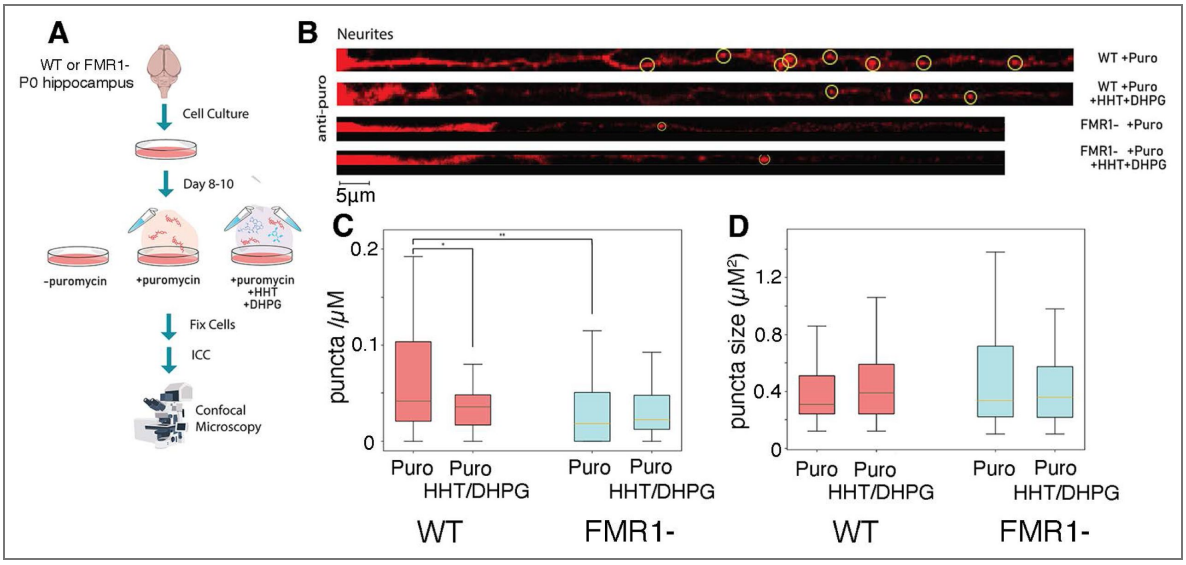

Figure 9. RPM of hippocampal cultures derived from WT and FMR1- mice.

A) Summary of the protocol for puromycylation HHT-Runoff and DHPG Reactivation on WT and FMR1- hippocampal culture. B) Representative confocal images for puromycylated ribosomes with or without HHT runoff and DHPG reactivation. Circle denotes puromycin puncta. No visible staining was seen in the absence of puromycin. Scale bar shown below. C) Quantification of RPM puncta density. Numbers are neurites/cultures. WT (42/5); WT DHPG (54/5), FMR1- (41/4), FMR1- DHPG (25/3). One way ANOVA $F(3,158)= 5.32$, $p< 0.005$) *, $p<0.05$ post-Hoc Tukey HSD test. Box and Whisker plot with line representing the median. D) Quantification of size of RPM puncta. WT 189/5; WT DHPG 171/5, FMR1- (118/4), FMR1-DHPG (48/3). Box and Whisker plot with line representing the median. One way ANOVA showed no significance ($P>0.05$).

reactivating stalled ribosomes (Graber et al., 2013; Graber et al., 2017). We replicated this result; DHPG significantly decreased the number of RPM puncta in WT cultures. However, DHPG had no significant effect on the decreased number of puncta in cultures from FMRP- mice (Fig. 9B,C). This is consistent with a loss of DHPG-sensitive RPM puncta in the absence of FMRP.

Discussion

Overall, there appeared to be no major changes in the biochemical composition of stalled ribosomes in the absence of FMRP (Fig. 1) or the state of the stalled ribosomes (Fig. 2). Most importantly, the places where ribosomes stall (peaks) are not changed in the absence of FMRP since the majority of peaks were present in both WT and FMR1- mice, and the RPFs from FMR1- brains still contained motifs in mRNAs previously shown to associate with FMRP (Fig. 8). Thus, the major conclusion of our study is that FMRP does not affect the locations at which neuronal ribosomes stall.

We did not observe major changes in a DEG analysis of RNA-seq between control and FMR1- mice in P5 brains, although some changes were observed using GSEA. This differs from many studies that do show differences in RNA-seq between these two groups at other stages of development or examining specific brain regions (Thomson et al., 2017; Sawicka et al., 2019; Kurosaki et al., 2022; Ntoulas et al., 2024). It is likely that our use of whole brains, a specific time point, and a relatively small number of biological replicates decreased our ability to see FMRP-related changes in mRNAs that are observed at a more cell-type-specific level and at different developmental times.

In the GSEA analysis of RPFs in the pellet (abundance) there were a number of gene sets that were decreased in the absence of FMRP. These gene sets were enriched in FMRP targets (Fig. 5). Indeed, if we focused just on the FMRP targets, there was a small but highly significant decrease in the relative abundance, occupancy and enrichment of these mRNAs in the absence of FMRP. Interestingly, the mRNAs identified in FMRP Clips could be divided into two classes based on whether they were also identified as mRNAs resistant to run-off. Only the FMRP targets that were also identified as mRNAs resistant to run-off showed increased occupancy compared to other mRNAs. mRNAs resistant to run-off that were not FMRP targets were still significantly decreased in abundance and enrichment, but unlike FMRP targets, loss of FMRP did not affect their occupancy. These results and the finding that peaks of RPFs are not affected by the loss of FMRP are consistent with FMRP not directly regulating stalling, but rather affecting whether stalled mRNAs are found in the pellet. This may be partly due to the role of FMRP in regulating the initiation of FMRP target mRNAs as only initiated mRNAs can be stalled. Indeed, there is considerable evidence that FMRP regulates initiation of a subset of mRNAs (Santini and Klann, 2014; Bagni and Zukin, 2019).

In contrast to the examination of the number of ribosomes and RBPs present in the ribosome clusters in the pellet, we did find a decrease in RPM puncta in hippocampal cultures and the remaining puncta were insensitive to DHPG (Fig. 9). FMRP contains a low complexity domain that allows phase separation to form spontaneously (Zhang et al., 2022). FMRP is subject to post translational modification by neuronal stimuli, such as mGluR-LTD (Niere et al., 2012; Khayachi et al., 2018) that reactivates translation from stalled ribosomes (Graber et al., 2013; Graber et al., 2017). Loss of FMRP leads to an increase in the amount of mGluR-LTD and removes the protein synthesis requirement for mGluR-LTD (Hou et al., 2006; Nosyreva and Huber, 2006). One possibility is that FMRP plays a role in retaining stalled ribosomes within RNA granules by maintaining their liquid-liquid phase, while post-translational modifications of FMRP participates in the controlled disassembly of these granules, enabling translational reactivation. In the absence of FMRP, premature disassembly of RNA granules may lead to premature production of proteins from mRNAs stalled in neuronal RNA granules.

The pellet and the RPM labeled granules are linked by the fact that both the ribosomes in the isolated clusters and in RPM puncta in hippocampal neurites can be puromycylated without dissociation of the puromycylated peptide, and in both puromycylation is less resistant to anisomycin (Graber et al, 2013; Anadolu et al, 2024; Fig. S9-1). However, while stalled

ribosomes are enriched in the pellet, it is not clear that only stalled ribosomes from neuronal RNA granules are present in the pellet. Moreover, it is not clear that all stalled ribosomes are sedimented in the pellet. FMRP may be more important in stabilizing ribosome clusters in RNA granules than for forming them. A better understanding of how ribosome clusters move in and out of RNA granules is required to address this issue in more detail.

Our previous results showed a larger protected fragment in RPFs from the pellet, but here we showed that this was due to incomplete nuclease protection. This incomplete digest was much more obvious at the entry site of the ribosome, than at the exit site, as the difference is cleavage is mainly at the 3'end of the protected mRNA (Anadolu et al., 2023)(Fig. 3). It is still unclear whether this is due to increased nuclease resistance of the mRNA near the entrance site of the ribosome due to secondary structures or just differences in nuclease accessibility to the region near the entrance site that is not neuronal specific. Further research on the mechanism of stalling may make this clearer.

Ribosomes containing secretory mRNA are stalled by the signal recognition protein and then co-translationally inserted into the ER. There is evidence that ribosomes attached to the ER can be transported in neuronal processes (Carter et al., 2020; Martin-Solana et al., 2024). Some local mRNAs hitchhike with mitochondria or endosomes (Fernandopulle et al., 2021). Differences in RNA composition between fraction 5/6 and the pellet may be due to increased sedimentation of these other forms of neuronal transport. Indeed, ribophorin, a rough ER protein that associates with ribosomes is enriched in the pellet compared to fraction 5/6 (Fig. 1). However, examination of our standard EM pictures show few examples of ribosomes attached to membranes (Carter et al., 2020; Martin-Solana et al., 2024) and the clustered ribosomes that make up most of the pellet and fraction 5/6 (Fig. 1) do not resemble ribosomes in transit in these other structures.

A major caveat of the present study is that the biochemical studies are only done at a single developmental point (P5 brains) and similarly, the hippocampal neurite studies use a single comparable time point. P5 brains were chosen due to their relative enrichment in neurons (Bandeira et al., 2009) and their lack of myelin. Myelin interferes with the sedimentation of ribosomal clusters (Khandjian et al., 2004; El Fatimy et al., 2016)and the detergents required to remove this interference also interfere with the sedimentation of ribosome clusters (Khandjian et al., 2004; El Fatimy et al., 2016) making comparable studies at later developmental time points not experimentally feasible at the present time. Thus, whether FMRP may play a more important role in determining stalling positions at later developmental time points cannot be ruled out.

Conclusions

We previously showed that the peaks of RPFs in ribosomes in the pellet contain sequences enriched in FMRP CLIP experiments (Anadolu et al., 2023). Here we show that this is independent of FMRP since the enrichment of these sequences is observed even when FMRP is lost. This suggests that, rather than FMRP driving the recognition of stalling sites, the sequences direct ribosome stalling, and that FMRP associates with stalled ribosomes. Moreover, FMRP does not affect anisomycin-resistant puromycylation of stalled ribosomes, nor does it alter the proteins associated with stalled ribosomes. There is a small decrease in the relative abundance, ribosome occupancy, and enrichment in the pellet of the FMRP clipped mRNAs (FMRP targets) suggesting that these mRNAs do have some specific relationship to FMRP that is independent of FMRP stalling these mRNAs. FMRP also plays a role in RNA granules containing stalled ribosomes since their number is decreased in the absence of FMRP, and the remaining granules are not reactivated by DHPG. We propose that FMRP is important for the regulated dissociation of the liquid-liquid phase neuronal RNA granules containing stalled ribosomes.

Methods

Purification of the RNA Granule-Enriched Fraction

All preparations used brains that were flash frozen using either liquid nitrogen or ethanol dry ice bath after dissection. Either three livers, five rat brains (Sprague Dawley; Charles River Laboratory) or 10 mouse brains (C57Bl/6) from WT and FMR1- mouse were used. All animals were 5d old. Samples were homogenized in either the previous (Anadolu et al, 2023) RNA Granule Buffer (20 mM Tris-HCl pH 7.4 (catalog #BP152-1, Thermo Fisher Scientific), 150 mM NaCl (catalog # BP358-212, Thermo Fisher Scientific), 2.5 mM $MgCl_2$ (catalog# M33-500, Thermo Fisher Scientific)) or high Mg^{2+} RNA Granule Buffer (20 mM Tris-HCl pH 7.4, 150 mM NaCl, 10 mM $MgCl_2$). These buffers were supplemented with 1 mM DTT (catalog #D9163, Sigma-Aldrich), and 1 mM EGTA (catalog # E8145 Sigma-Aldrich) for homogenization. The homogenate was centrifuged 15min in a Thermo Fisher Scientific T865 fixed-angle rotor at 6117 x g at 4 °C to separate debris, such as lipid and extracellular matrix, from the ribosomes. The supernatant was collected with some set aside as starter fraction. The rest of the supernatant was then clarified with 1% IGEPAL CA-630 (catalog #04693132001, Roche) for 5 min at 4 °C Sucrose solution was produced by suspending sucrose (catalog #8550, Calbiochem) with RNA Granule buffer. The samples were loaded onto a 60% sucrose pad in a Sorvall 36 ml tube (Kendro, catalog #3141, Thermo Fisher Scientific) and centrifuged at 56,660 x g for two hours in AH-629 swing-bucket rotor to retrieve the ribosomes. The ribosomes were resuspended in RNA Granule buffer then reloaded onto 15%-60% sucrose gradient and centrifuged at 56,660 x g for 45 min. Each fraction was 3.5 ml and collected from the top.

Immunoblotting and quantification of enrichment

For immunoblotting, the pellet and fraction 5/6 were ethanol precipitated and resuspended with 1x sample buffer and RNA Granule buffer. The samples were loaded onto 10%, 12% or 15% acrylamide gel according to the observed protein sizes. The gel was either stained with Coomassie Brilliant Blue to look at the protein distribution or transferred onto a 0.45um nitrocellulose membrane (catalog #1620115, Bio-Rad) for immunoblotting. The transferred membranes were stained with Ponceau and imaged. Then, the membranes were blocked with 5% BSA (catalog # A9647, Sigma Aldrich) in Tris-buffered saline with Tween before incubation with primary antibodies— rabbit anti-s6 (1:10,000) (catalog #2217, Cell Signaling Technology), rabbit anti-FMRP (1:500)(catalog #4317, Cell Signaling Technology), rabbit anti-UPF1 (1:10,000)(catalog #ab133564, Abcam), mouse anti-Stau2 (1:1000)(catalog #MM0037-P, MediMabs), anti-eEF2 (1:1000)(catalog #2332S, Cell Signaling Technology), rabbit anti-Pur-alpha (1:1000)(catalog #ab79936, Abcam), rabbit anti-ZBP1 (1:500)(catalog # NBP1-7685 Novus Biologicals, rabbit anti-TIA1 (1-1000)(Catalog #12133-2-AP Proteintech), rabbit anti-hNRPA2B1 (1:1000)(catalog #NB120-6102), mouse monoclona anti-ribophorin (1:200)(Catalog #sc-48367 Santa Cruz Biotechnology) and anti-mouse puromycin (1:1000)(catalog #ab2619605, Developmental Studies Hybridoma Bank). Membranes were washed with TBS-T after incubation. HRP-conjugated secondary antibodies such as anti-rabbit HRP (1:10,000)(catalog #31460, Thermo Fisher Scientific) and anti-mouse HRP (1:10,000)(catalog #31430, Thermo Fisher Scientific) were incubated with the membranes for detection. ECL reaction was performed for imaging, and the images were scanned and quantified by ImageJ software. The single band for each protein was selected and quantified using ImageJ's Gel analysis Macro. For S6, the levels in the pellet and fraction 5/6 were directly compared based on the fraction of the samples loaded on the gel . For other proteins, the levels in the pellet and fraction 5/6 were first calculated based on the fraction of the samples loaded on the gel and then normalized to the relative S6 levels found in the pellet and fraction 5/6 from this preparation to provide a RBP/ribosome ratio. The enrichment for the pellet was determined by dividing this normalized value between the pellet and fraction 5/6. . A two tailed, one sample t-test was performed between the enrichment and 1 with Bonferroni correction for multiple T-tests to test for significant enrichment. A two tailed, Welch's t-test was performed between the enrichment of WT and FMR1- with Bonferroni correction for multiple T-tests to observe the differences between the two groups.

UV absorbance

2 µL of each fraction was measured using Nanoblot 1000 Spectrophotomer (Thermo Fisher Scientific). Averages of the value between three independent experiments from WT and FMR1-mice were used.

Inhibition of Puromycylation by Anisomycin

The liver ribosomes were extracted from P5 Spraque Dawley rats through the identical method as the RNA Granules, but without the last spin since liver does not contain appreciable levels of ribosomes in the pellet. All ribosomal fractions used were incubated for 5 min in 1) RNA Granule buffer 2) 100µM puromycin (catalog# P7255, Sigma Aldrich), or 3) 100µM puromycin and 100µM anisomycin (catalog# A9789, Sigma Aldrich). The samples were then ethanol precipitated, immunoblotted and quantified via the method stated above. The percentage of puromycin resistant to anisomycin inhibition were calculated by dividing anti-puro signal from the puromycin and anisomycin added sample against the anti-puro signal from the puromycylated sample within each replicate.

Digestion and extraction of the monosomes

Fraction 5/6 samples were loaded onto a 60% sucrose pad and centrifuged to concentrate the samples, while the pellet samples were resuspended from the pellet using 1 ml of normal or high $MgCl_2$ Granule buffer. For normal nuclease treatment groups, 1µl of RNAase I (100U/µ l; catalog #AM2294, Thermo Fisher Scientific) was administered to the ribosomes and rotated at 4°C for 30min. Then, 4µl of SuperaseIN (20U/µl; catalog # AM2969, Invitrogen) was added to the solution to halt the reaction. The samples are then loaded onto 15% to 60% sucrose gradient and centrifuged at 56,660 x g for 45 minutes to retrieve the monosomes from fraction 2 and 3. For high nuclease treatment group, RNAse I (10 U/µl, catalog #N6901K, Epicentre) was adjusted to the concentration of ribosomes via the A260 read from the Nanodrop. The OD obtained from the A260 read equals 6 unit. In other words, the amount of nuclease (µl) added equals A260 * 6 (U)/ 10 (µl/U). In addition, the samples are incubated at room temperature for 30 min rather than at 4 °C. Then, 6µl of SuperaseIN were added to halt the reaction. The samples were then spin at 68,000 x g for 3hrs on a Beckman tabletop ultracentrifuge to concentrate the monosomes, which pellets. The RNA from the monosomes was extracted using the trizole chloroform method followed by isopropanol precipitation to concentrate the samples. The samples were loaded onto Urea gel (catalog # EC68852Box, #EC68752Box, #EC62152Box, ThermoFisher) to select for RPF size. Segments between 25b and just above 40b were excised and retrieved to account for the possible longer fragments of the RPFs. The excised gels were frozen on dry ice for 30 minutes and then thawed overnight at room temperature. The RNA was extracted again with trizole chloroform extraction.

Linker Ligation

The protocols follow improvements in RPF ligation (McGlincy and Ingolia, 2017). The concentration from the RNA footprint was calculated from Bioanalyzer small RNA kid (catalog # 5067-1548, Agilent). An equal amount of RNA was calculated and transferred to a new tube for each sample to ensure each sample has a relatively equal amount after pooling. 3 different linkers (NI-810, NI-811, BI-812) were attached to each of the replicates. The samples were first dephosphorylated with T4PNK linker (catalog # M0351L, NEB), and then pre-adenylated linkers are attached through T4 Rnl2 (catalog # M0351L, NEB). The linked RNA was purified through excision of urea gel between 50bp and 70bp. Samples with the same variables were then pooled together with their gel fragment combined. The RNA was extracted from the gel with the steps stated previously containing all three replicates, followed by Reverse transcription. MyOne Streptavidin C1 DynaBeads (catalog#65001, ThermoFisher) was used for rRNA depletion. Lastly, PCR was performed. The samples were sequenced through the McGill University Genome Center on NovaSeq S1/2 flow cells.

RPF and RNA-seq data analysis

The raw reads were processed using Cutadapt (version 2.10), where sequences were trimmed to remove adapters and low-quality bases. Subsequently, demultiplexed each pooled reads runs using UMI barcodes (ID1=ATCGT, ID2=AGCTA and ID3=CGTAA). Additionally, options were used to trim N bases (--trim-n), discard sequences shorter than 18 bases (--minimum-length=18), allow a minimum overlap of 5 bases (--overlap=5), and omit insertions or deletions (--no-indels). Untrimmed reads were discarded, and trimming logs were saved for quality control. Reads mapping to non-coding RNAs (ncRNAs) and ribosomal RNAs (rRNAs) were filtered out using Bowtie2 (version 2.3.5), aligning the reads against rRNA and ncRNA sequences from the Mus musculus reference (GRCm38, Ensembl release 102). The Bowtie2 parameters were set to maximize sensitivity (--very-sensitive). Unmapped reads were further aligned to the Mus musculus genome (GRCm38, Ensembl release 102) using the STAR aligner (version 2.7.8a). The output was generated as transcript coordinate-sorted BAM files (--outSAMtype BAM SortedByCoordinate --quantMode TranscriptomeSAM). PCR duplicates were identified and marked using *Picard MarkDauplicates* (version *2.26.6)*. These duplicates were then removed using *samtools* (version 1.19.2). Further, raw counts were obtained using featurecounts (version 2.2.0).

For RPKM and all DEG analysis, non-protein coding genes were removed. RPKM, reads per kilobase per million mapped reads, were calculated for abundances, which normalized the raw counts against gene length and total count. Occupancy for individual groups were calculated through performing DEG analysis between pellet raw count replicates and whole brain RNA-seq replicates, and enrichment for individual groups were calculated through performing DEG analysis between raw count pellet replicates and raw count fraction 5/6 replicates. For comparison between WT and FMR1- groups, DEG Analysis was calculated as follow: abundances, raw count WT vs raw count FMR1- ; occupancy, raw count WT pellet divided by whole brain RNA-seq vs raw count FMR1- pellet divided by whole brain RNA-seq, enrichment, raw count WT pellet divided by raw count WT fraction 5/6 vs raw count FMR1- pellet divided by FMR1-KO fraction 5/6..

The Differential Expression Gene Analysis was performed via R studio packages in *edgeR* from Bioconductor adapted for RNA-seq (Wu et al., 2021). Data were normalized for library size differences and filtered to remove lowly expressed genes. Results were ranked and evaluated based on adjusted p-value (FDR), which was calculated through the Benhamini-Hochberg method. To visualize sample clustering and data quality, Principal Component Analysis (PCA) was performed on log-transformed counts-per-million (CPM) values using the `stats` and `edgeR` packages low expression gene was filtered and normalized. For GSEA, resulting gene lists were ranked and processed for Gene Set Enrichment Analysis (GSEA) using the fgsea package against MSigDB C5 (GO) mouse gene sets. Pathway enrichment was restricted to sets containing 10–500 genes, with significance prioritized by the Benjamini-Hochberg adjusted p-value. GO Enrichment Analysis was performed with clusterprofiler (Wu et al., 2021) and org.Mm.eg.db from Biomanager using R studio (Yu, 2024). Comparison to data online was performed via jupyter notebook and graphed by *boxplot* in *matplotlib*. The significance of each dataset comparison was done through performing t-test between the overlapped gene in our data and non-overlapped genes through the *statistics* function from python. The p-value was Bonferroni corrected.

We used transcript coordinate Bam files for peak analysis. Regions of the mRNA that have an abundant amount of RPFs were referred to as peaks (Anadolu et al., 2023). The peaks previously were selected through marking the inflection point within the abundances of RPFs. Here, we identify the highest point (zenith) in the peak after mapping RPFs to transcripts. To be identified as a peak, the zenith of an abundance site for the reads must be 4x higher of the average of the total transcript. Moreover, this zenith must be detected in all the biological samples (zenith within 6 nucleotides for each replicate). We first determine total peaks in all six samples (WT and FMR1-) and then determined peaks that were in all WT samples, but not in FMR1- samples (WT peaks; peaks lost in the absence of FMRP) and peaks that were present only in the FMR1- samples, but not in any WT samples (FMRP peaks).

For identification of motifs in the peaks, the zenith was extended on both sides by 17nt. Motif occurrences in the peaks were identified using FIMO from the MEME suite (Bailey et al., 2015) and universalmotif (Tremblay, 2024). Percentage peaks with FXS related motifs were identifying only the positive strand and limiting the score, or log-likelihood ratio, to 5, and normalizing against the total peaks. Biopython was utilized to convert peak sequences to amino acids.

Cryo-electron microscopy

The purified fractions were treated with nuclease as described (Anadolu et al., 2023) before being applied to the electron microscopy grids. The samples were applied to the grid in buffer containing 20mM Tris-HCl, pH 7.4; 150 mM NaCl; 10 mM $MgCl^{2+}$, and they were applied at a concentration of 180 nM. Cryo-EM grids (c-flat CF-2/2-2C-T) used for these samples were washed in chloroform for two hours and treated with glow discharge in air at 15 mA for 20 seconds. A volume of 3.6 µL was applied to the grid before vitrification in liquid ethane using a Vitrobot Mark IV (Thermo Fisher Scientific Inc.). The Vitrobot parameters used for vitrification were blotting time 3 seconds and a blot force +1. The Vitrobot chamber was set to 25 °C and 100% relative humidity.

All datasets were collected at FEMR-McGill using a Titan Krios microscope operated at 300 kV and equipped with a Gatan BioQuantum LS K3 direct electron detector. The software used for data collection was SerialEM (Schorb et al., 2019). Images were collected in counting mode at a nominal magnification of 81,000x, producing images with a calibrated pixel size of 1.09 Å. Movies for all datasets were collected using 30 frames with a total dose of 40 $e^{-}/Å^{2}$.

Image processing

All the image processing steps were done using cryoSPARC v4.5 software (Punjani et al., 2017). A total of 10,866 cryo-EM movies were corrected for beam-induced motion correction using Patch Motion Correction using default settings that included using information up to 5Å resolution when aligning frames, a B-factor of 500 and a 0.5 calibrated smoothing constant applied to the trajectories. CTF parameter estimation was done using Patch CTF estimation with default settings. The minimum and maximum resolution considered to estimate the CTF parameters were 25 Å and 4 Å, and the minimum and maximum defocus values were set up at 1,000 and 50,000 Å. The corrected micrographs were then curated by Manually Curate Exposures. For the particle-picking step, the Blob Picker program was first applied to 2,000 obtained micrographs using a circular blob with a minimum and maximum particle diameter of 200 Å and 480 Å. The maximum resolution considered during picking was 20 Å. The angular sampling used was 5 degrees, and the minimum particle separation distance was 0.5 (in units of particle diameters). The picked particles were extracted with a box size of 448 pixels, which was reduced to 112 pixels, and then subjected to 2D classification to generate the 2D templates for subsequent Template Picker using the 2,000 micrographs. In the 2D Classification step, we requested 50 classes and we selected 0.85 and 0.99 as inner and outer window radius. The maximum resolution considered in the images was 9 Å, and we used an initial uncertainty factor of 2. The remaining settings were used with their default parameters. The particles obtained from the Template Picker were curated again by 2D classification to remove the bad particles using the same job parameters. The curated particles were selected and used to train a model using Topaz (Bepler et al., 2019) with default settings, including a minibatch size of 128 and an expected number of particles of 165 per micrograph. The trained model was then used to pick particles from all the micrographs. The selected particles underwent 2 cycles of 2D Classification to remove junk particles. The obtained particles were then subjected to the subsequent particle curation step, which combined Ab-initio Reconstruction and Heterogeneous Refinement programs using default settings. For the Ab-Initio step, we selected 0.85 and 0.99 as inner and outer window radius, requested 3 classes and a maximum and minimum resolution to consider of 35 Å and 12 Å. All other parameters for this routine were used with the default settings and values. The three initial Ab-initio models generated were subsequently used in a Heterogeneous Refinement using default parameters to separate the particles into multiple

classes. The particles assigned to the class with unidentifiable features were discarded, whereas the particles assigned to reconstructions with ribosomal features were merged for subsequent processing. The total number of good particles after particle curation was 890,644.

To explore the structural heterogeneity, the curated set of particles was used to generate a consensus map with Non-Uniform Refinement at default settings and C1 symmetry. The aligned particles were then subjected to 3D Variability Analysis requesting 3 orthogonal principal modes and the subsequent 3D Variability Display 3D job was ru in cluster mode with all settings at default values. The number of clusters requested across experiments, ranging from 3 to 5.

Results were filtered at 9 Å. Overall, we performed two rounds of the 3D Variability Analysis combined with 3D Variability Display to address sample heterogeneity. Resulting maps from the exhaustive 3D classification were visually inspected in (Pettersen et al., 2004; Pettersen et al., 2021) and groups of particles representing similar structural features were merged. To obtain high-resolution structures, the particles from each class were extracted with a box size of 448 pixels and refined with Non-Uniform Refinement. The refinement jobs were run under default settings with C1 symmetry, optimized per-particle defocus, optimized per-exposure group CTF parameters and options 'Fit Spherical Aberration', 'Fit tetrafoil' and 'Fit anisotropic Magnification' activated. To improve local resolution, Local Refinement was performed under default settings to refine the two subunits (40S and 60S) independently for all the classes. Particle Subtraction run under default settings was used before Local Refinement to subtract the signal from the particle stacks that will not be used for Local Refinement. Composite maps were obtained by aligning them to the consensus maps of the 80S ribosome and merging the 60S and 40S cryo-EM maps from local refinement using the 'vop add' command in Chimera.

Average resolution estimation and local resolution analysis were done with cryoSPARC using the gold-standard approach (Henderson et al., 2012). For each map, we calculated the following FSC plots: 'No mask': the raw FSC calculated between two independent half-maps reconstructed from the data and no masking applied. 'Loose': FSC calculated after applying a loose soft solvent mask to both half maps. The loose mask is calculated by thresholding the density map at 50% of the maximum density value. The resulting volume is dilated to create a soft mask. Voxels in the mask within 25 angstroms of the thresholded region receive a mask value of 1.0. Voxels between 25 and 40 angstroms fall off with a soft cosine edge, and voxels outside 40 angstroms receive a value of 0.0. 'Tight': FSC calculated after applying a tight soft solvent mask to both half maps. The tight mask is calculated by the same procedure as the loose mask, except that the dilation distances are 6 angstroms for the value 1.0 distance and 12 angstroms for the value 0.0 distance. 'Corrected': FSC curve calculated using the tight mask with correction by noise substitution (Chen et al., 2103). In brief, the two half maps have their phases randomized beyond a certain resolution, then the tight mask is applied to both, and an FSC is calculated. This FSC is used along with the original FSC before phase randomization to compute the corrected FSC. This accounts for correlation effects induced by masking. The resolution at which phase randomization begins is the resolution at which the no-mask FSC drops below the FSC = 0.143 criterion. Cryo-EM map visualization was performed in UCSF Chimera and Chimera X (Pettersen et al., 2004; Pettersen et al., 2021).

Ribopuromycylation Assay

WT mouse and FMR1- mouse hippocampal neurons were dissected from P0 mouse and cultured on to poly-L-lysine (PLL)-coated 18mm coverslips as previously described (Langille et al., 2019). The hippocampal neurons were incubated with Neurobasal media supplemented with 1% (vol/vol) N2 and penicillin/streptomycin, 2%(vol/vol) B27 and 0.5 mM GlutaMAX (Life Technologies). Treatment groups: +puro (puromycin), -puro, +puro + anisomycin, +puro +HHT (homoharringtonine), and +puro + HHT + DHPG (S)-3,5-Dihydroxyphenylglycine) were assigned to cells and added to the culture on day 8. Cells that were assigned to HHT or HHT + DHPG conditions were preincubated with supplemented neural basal media as stated above with 5μM HHT (catalog # 1416, Tocris Bioscience) or with 5μM HHT and 100μM DHPG (catalog # 0805, Tocris Bioscience) for 15min in 37°C to ensure sufficient time for ribosomes to runoff and for DHPG to reactivate stalled ribosomes. The control +puro, - puro, and + puro +Aniso groups were incubated with

supplemented neural basal media. The solution was then removed from all groups and replaced with new supplemented neural basal medium for the control group and supplemented neural basal medium with 100µM Puromycin or 100µM Puro and 100µM Anisomycin. All groups were incubated at 37 °C for 5min similar to previous experiments (Graber et al, 2013; Langille et al 2019). The cultures were then placed on ice and washed with HBS supplemented with 0.0003% digitonin for 2min, followed by 3x wash with HBS. The cultures were then placed at room temperature and fixed with 4% paraformaldehyde for 30 min. Upon completion, the cell cultures were washed with PBS three times, sealed in the 1x PBS, and placed at 4°C till immunocytochemistry.

Immunocytochemistry

Cultures were treated with 0.1% Triton-X 100 with 30% sucrose in PBS for 10min to allow for permeabilization of cell membrane followed by 15min of quench solution (55mM ammonium chloride in 1x PBS). The cultures were then washed in 1xPBX for three times before blocking with 1% BSA in PBS for 30min. The cultures were then incubated with primary antibody solution (1:1000 mouse anti-puromycin (DSHB Hybridoma Product PMY-2A4)) in 1% BSA and 1xPBS for 1hour. The primary antibody solution was then removed, and the cultures were then washed 3 times with 1xPBS. Secondary antibody solution (anti-mouse 1:1000 Alexa Fluor 745) was then added to the cultures and incubated for 1hour. The secondary antibody solutions were then removed, and the cultures were washed 3 times with 1xPBS. The culture-containing coverslips were then removed and mounted using 10µL of Dako mounting medium. The coverslips were stored in the dark before imaging.

Confocal Microscopy

Cells were imaged using a Zeiss LSM-900 confocal microscope with a 63x oil immersion objective. The images were then assigned numbers and randomized to lower potential biases. ImageJ was used to straighten the neurites.

Quantification of RPM

Only cells with straightened neurites over 75 µm were used. The person doing the quantification was blind to the treatment or genotype. The images were converted to 8 bits and then thresholded at a minimum of 180/256 pixel intensity although there was a manual component to this quantification based on the relative brightness of the image. The analyze particle Macro of Image J was used to identify puncta with size criteria of 0.15 to 2 μm^2 and circularity of 0.4-1.0. Only puncta>50 µm from the soma were considered for this analysis.

Data availability

The cryo-EM maps obtained in this study have been deposited in the Electron Microscopy Data Bank (EMDB), and the accession codes are detailed in Supplemental Table 4-1. All sequences are available in the GEO database (GSE291701).

Supplemental figures and table

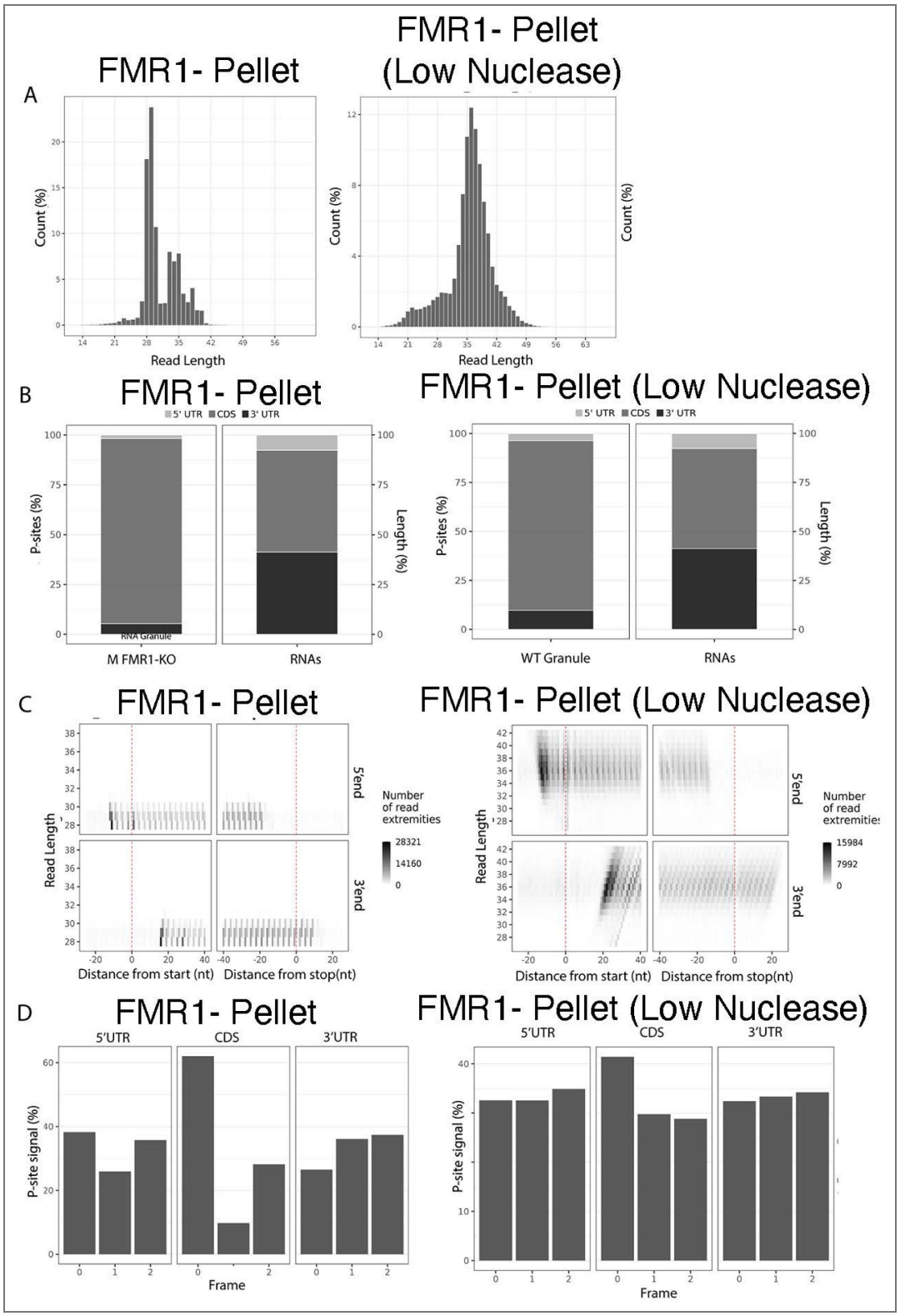

Figure S3-1. Higher Nuclease reduces size of RPFs in FMR1- pellet . A) Size distribution of normalized footprint reads from the FMR1- Pellet fraction under standard or low nuclease treatment. B) Representative image for read coverage for the FMR1- Pellet fraction either with standard or low nuclease treatment, UTR, untranslated region; CDS, coding sequence for both RPFs and RNA-seq libraries. C) Representative image for the number of read extremities (shading) for each read length (Y-axis) based on the distance from start(left) to stop(right) with the 5'

end (top) and 3’ end (bottom) for the FMR1- pellet fraction with either standard or low nuclease treatment. E) Representative image for the periodicity statistics for RPFs in different regions of the mRNA for standard or low nuclease treatment. Although the representative images above included only one replicate, similar results were observed across all three replicates.

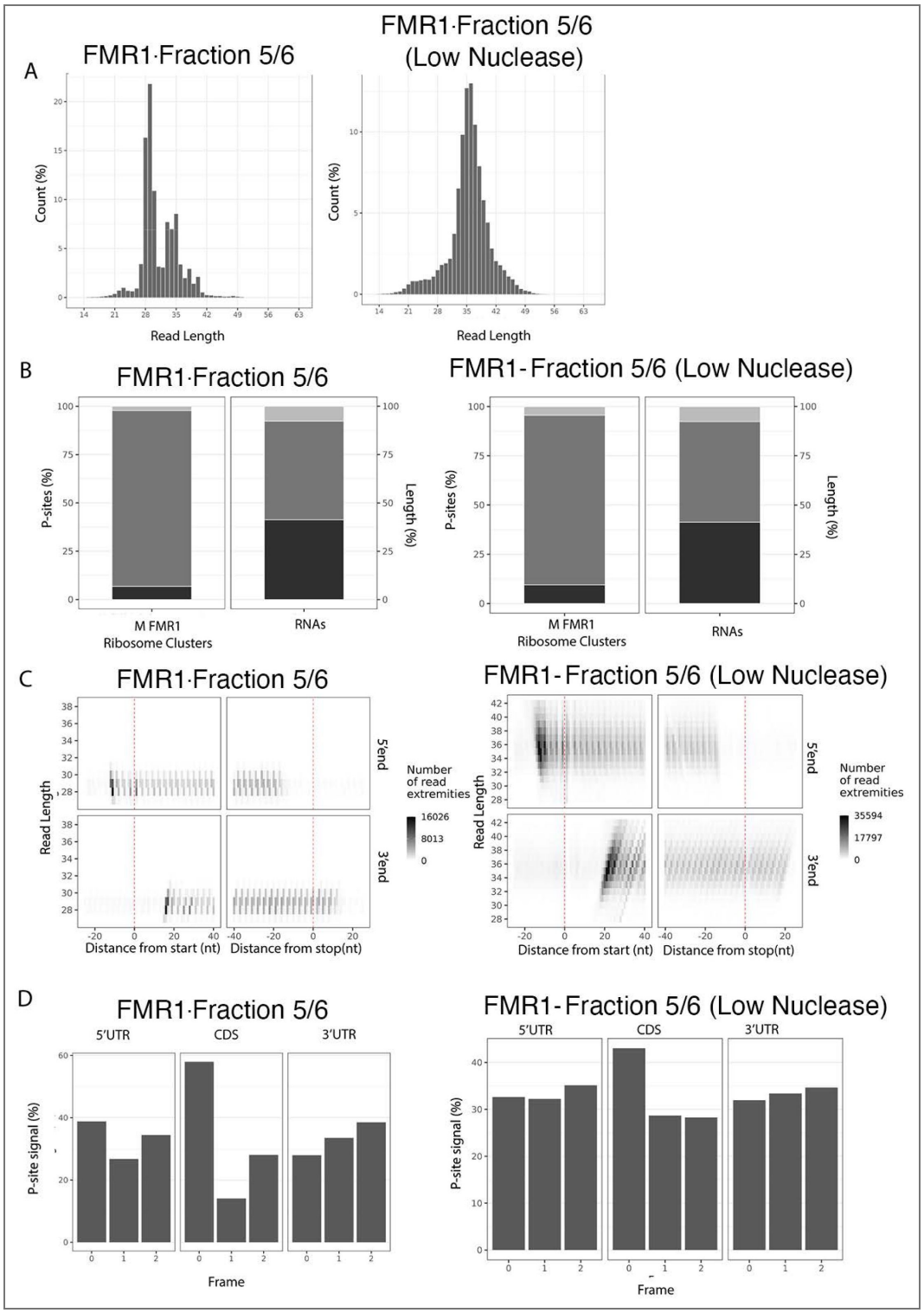

Figure S3-2. Higher Nuclease reduces size of RPFs in FMR1- Fraction 5/6

A) Size distribution of normalized footprint reads from the FMR1- fraction 5/6 under standard or low nuclease treatment. B) Representative image for read coverage for the FMR1- fraction 5/6 either with standard or low nuclease treatment, UTR, untranslated region; CDS, coding sequence for both RPFs and RNA-seq libraries. C) Representative image for the number of read extremities (shading) for each read length (Y-axis) based on the distance from start(left) to stop(right) with the 5' end (top) and 3' end (bottom) for the FMR1- fraction 5/6 with either standard or low nuclease treatment. E) Representative image for the periodicity statistics for RPFs in different regions of the mRNA for standard or low nuclease treatment. Although the representative images above included only one replicate, similar results were observed across all three replicates.

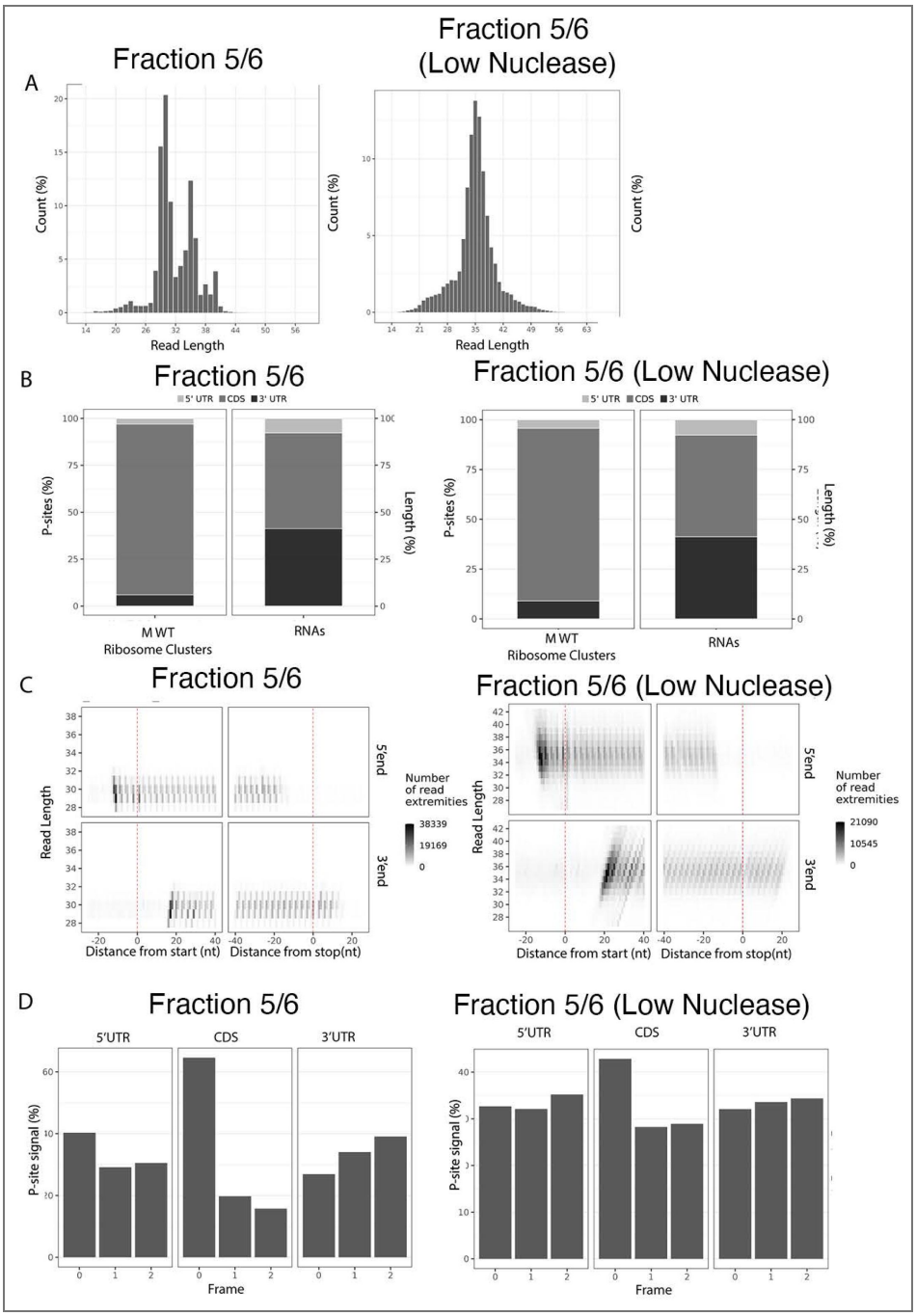

Figure S3-3. Higher Nuclease reduces size of RPFs in WT fraction 5/6.

A) Size distribution of normalized footprint reads from the WT fraction 5/6 under standard or low nuclease treatment. B) Representative image for read coverage for the WT fraction 5/6 either with standard or low nuclease treatment, UTR, untranslated region; CDS, coding sequence for both RPFs and RNA-seq libraries. C) Representative image for the number of read extremities (shading) for each read length (Y-axis) based on the distance from start(left) to stop(right) with the 5′ end (top) and 3′ end (bottom) for the WT fraction 5/6 with either standard or low nuclease treatment. E) Representative image for the periodicity statistics for RPFs in different regions of the mRNA for standard or low nuclease treatment. Although the representative images above included only one replicate, similar results were observed across all three replicates.

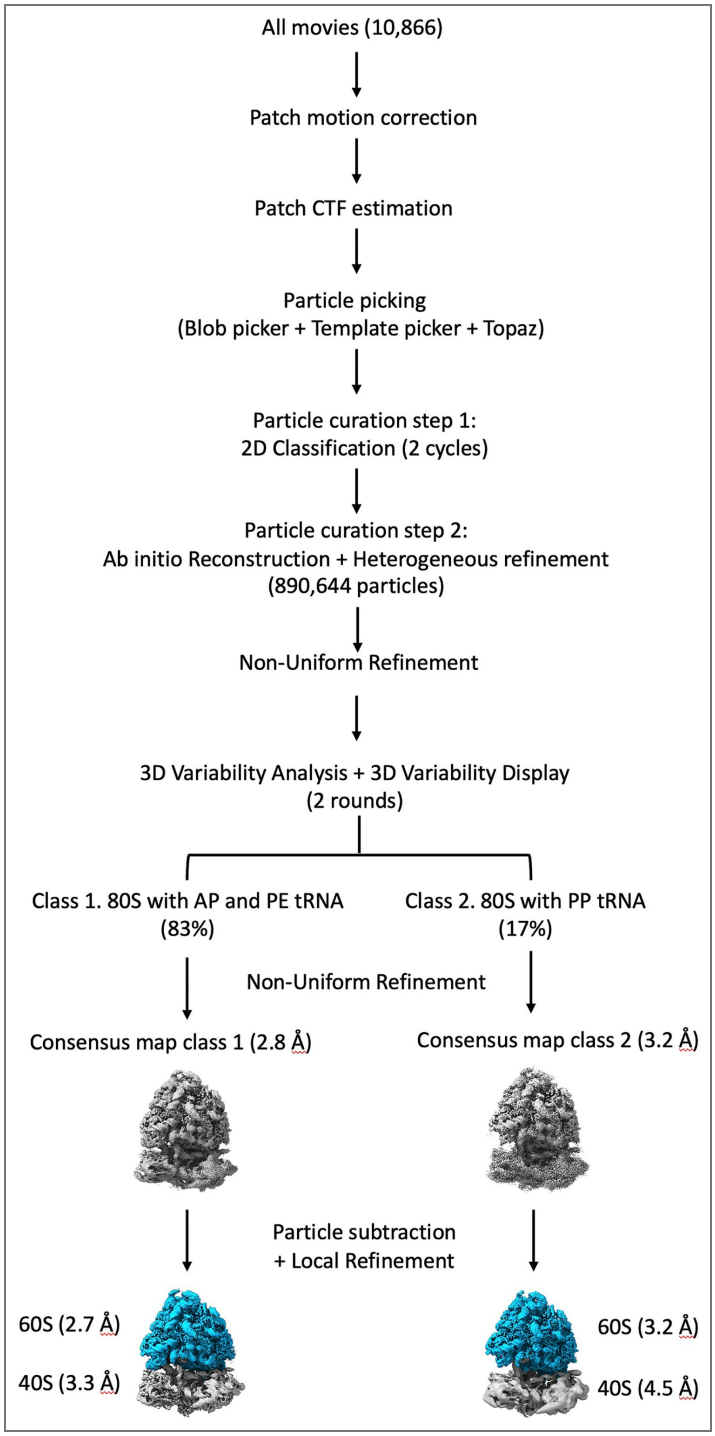

Supplementary Figure S4-1. Single particle analysis image processing workflow.

The cryo-EM dataset obtained from the pellet fraction after purification in high-magnesium buffer and RNase I treatment was subjected to the image-processing workflow shown in the figure. The diagram shows the main image processing steps performed on this dataset and the two main ribosome populations identified by the image classification approaches. The resolutions for the consensus maps and for each subunit in the maps obtained through local refinement are also indicated.

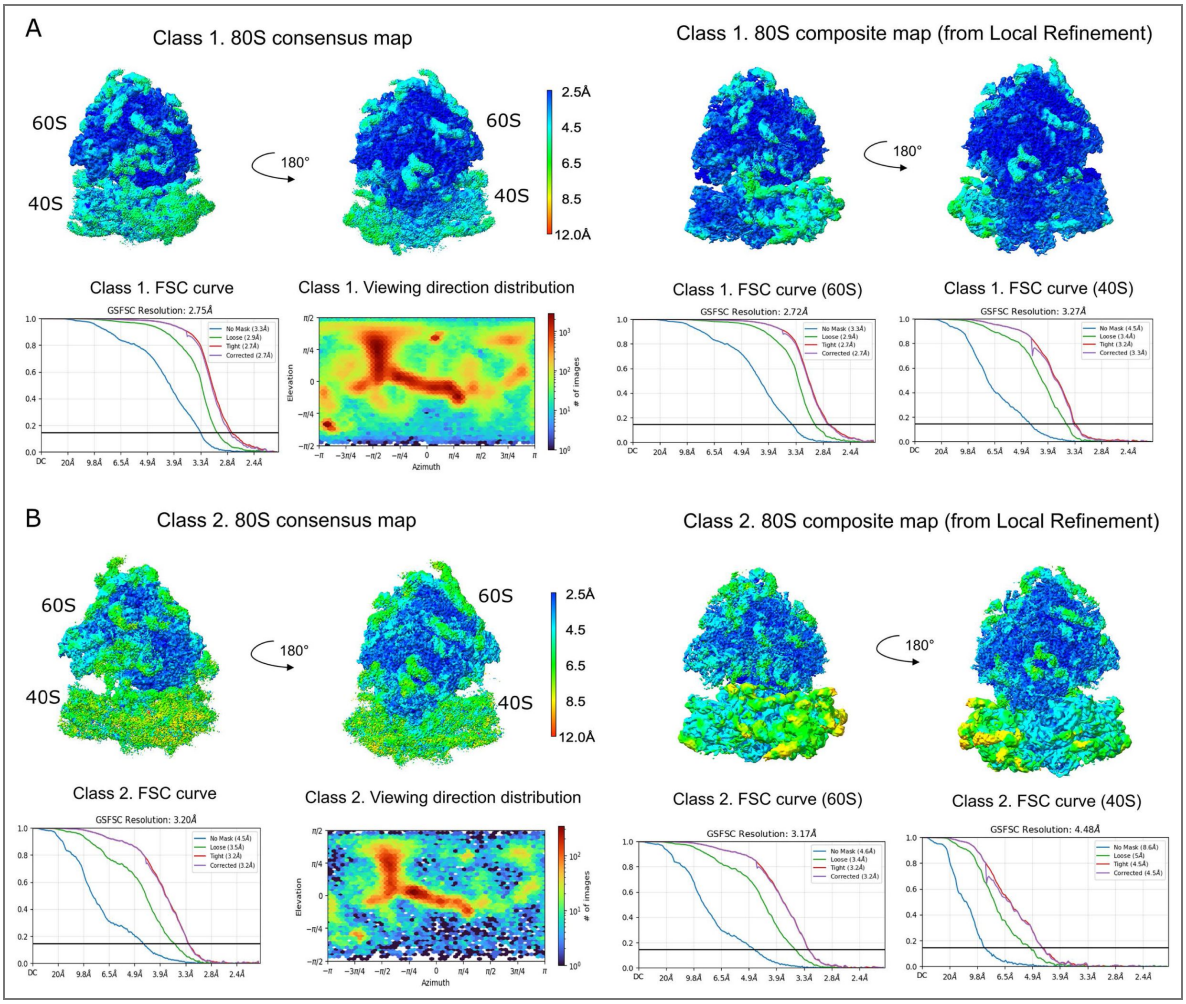

Supplementary Figure S4-2. Resolution analysis of the two major classes of 80S ribosomes in the Granule Fraction purified under high magnesium conditions.

Consensus cryo-EM maps (left panels) were initially calculated for class 1 (A) and class 2 (B) from the RNase I-treated pellet Fraction purified under high magnesium buffer conditions. These maps were subsequently refined by local refinement by dividing the 80S ribosome into two major bodies, the 60S and the 40S particles. The top panels in (A) and (B) show the local resolution analysis of the 80S consensus and composite maps obtained using local refinement. Maps are colored according to their local resolution using the color coding indicated in the scale bars. The Fourier shell correlation (FSC) curves for the consensus maps and each one of the subunits after the maps were subjected to local refinement are shown for class 1 and 2. For each class, we show the following FSC plots: 'No mask', 'Loose', 'Tight', and 'Corrected'. These plots were calculated as described in the Methods section. We used a FSC threshold of 0.143 to report the overall resolution of the maps. The 'Viewing direction distribution' plot in panels (A) and (B) show the orientation distribution of the particles contributing to the cryo-EM map for each one of the classes. These plots are 2D histograms that show the number of particles with a viewing direction at a particular elevation/azimuth bin. The number of particles can be inferred by the color code scale bar to the right of each plot.

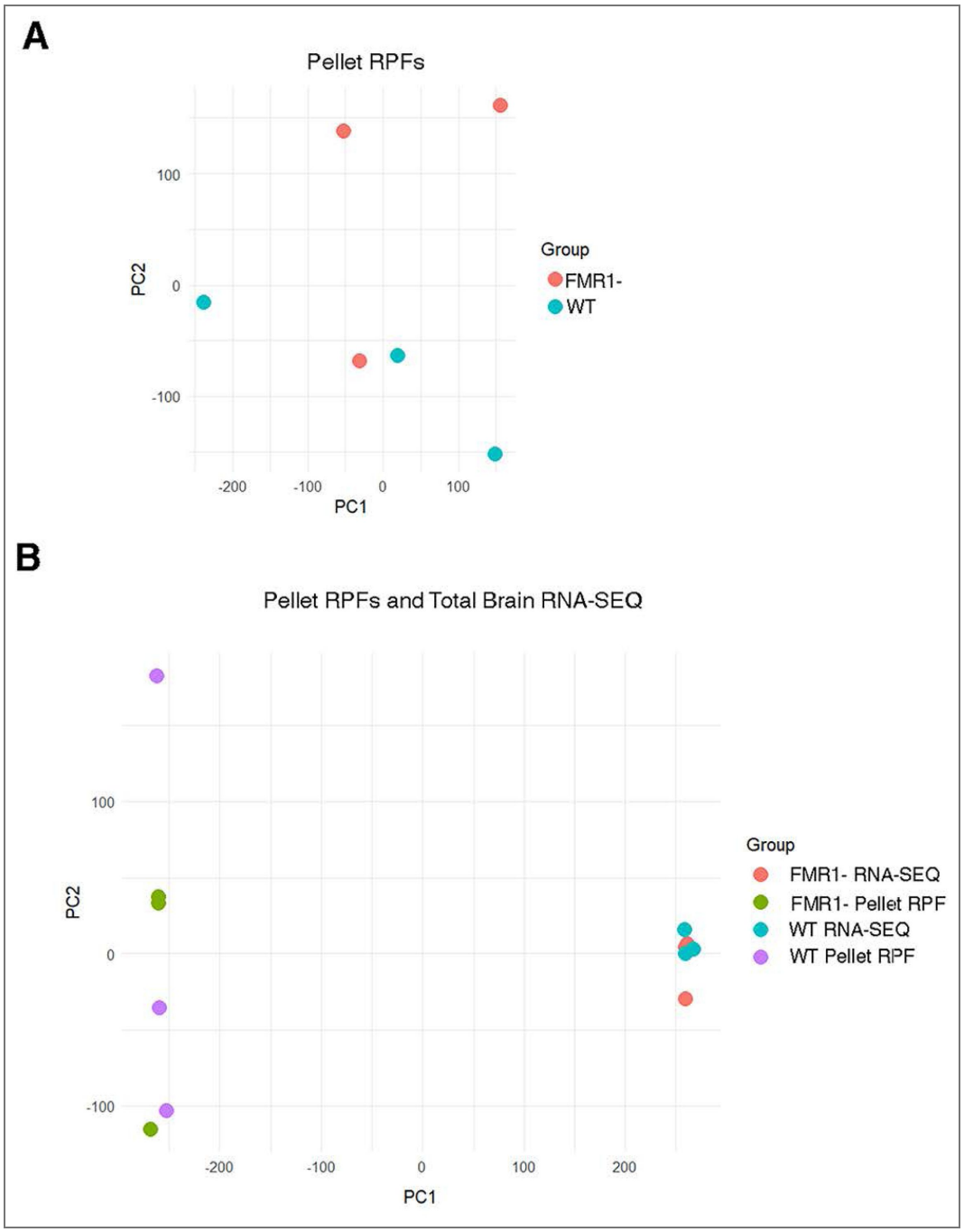

Supplemental Figure 5-1. PCA Analysis.

A) PCA analysis of Pellet RPFs from WT and FMR1-replicates. B) PCA analysis of Pellet RPFs and RNA-SEQ samples from WT and FMR1-replicates.

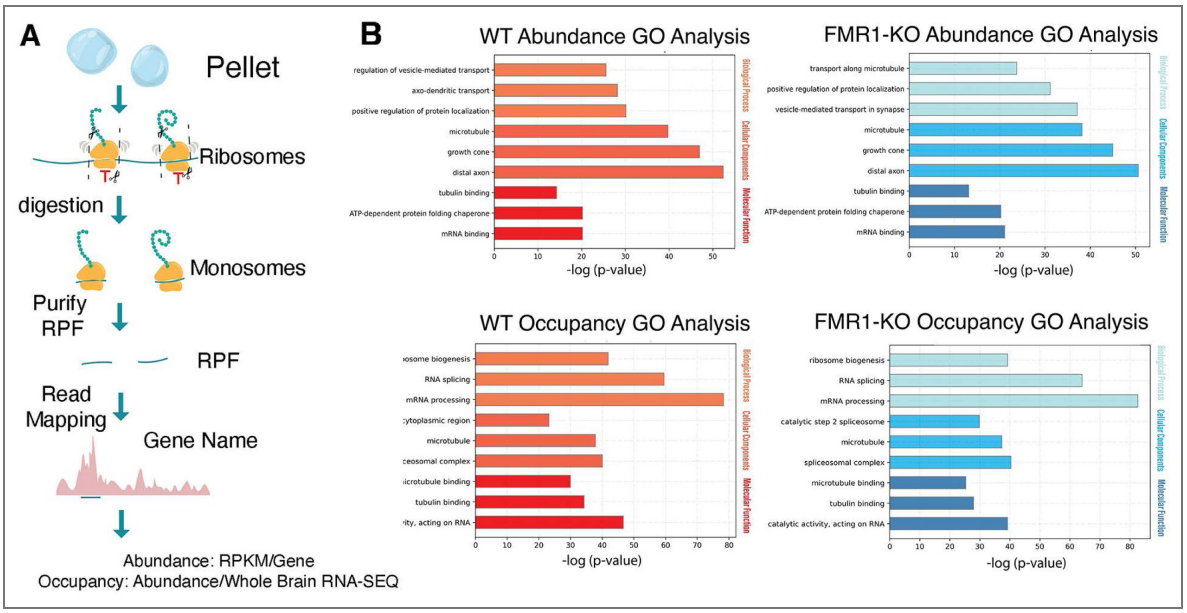

Supplemental Figure S5-2. Assessment of RPF abundance, occupancy and enrichment in Pellets of WT and FMRI- mice.

A) summary of protocol to generate RPF abundance, occupancy and enrichment. B) GO terms of the WT pellet (left) and FMR1- pellet (right)for abundance (top) and occupancy (bottom) For each graph, GO terms from the top 500 genes: Biological Function (top), Cellular Components (middle), and Molecular Function (bottom).

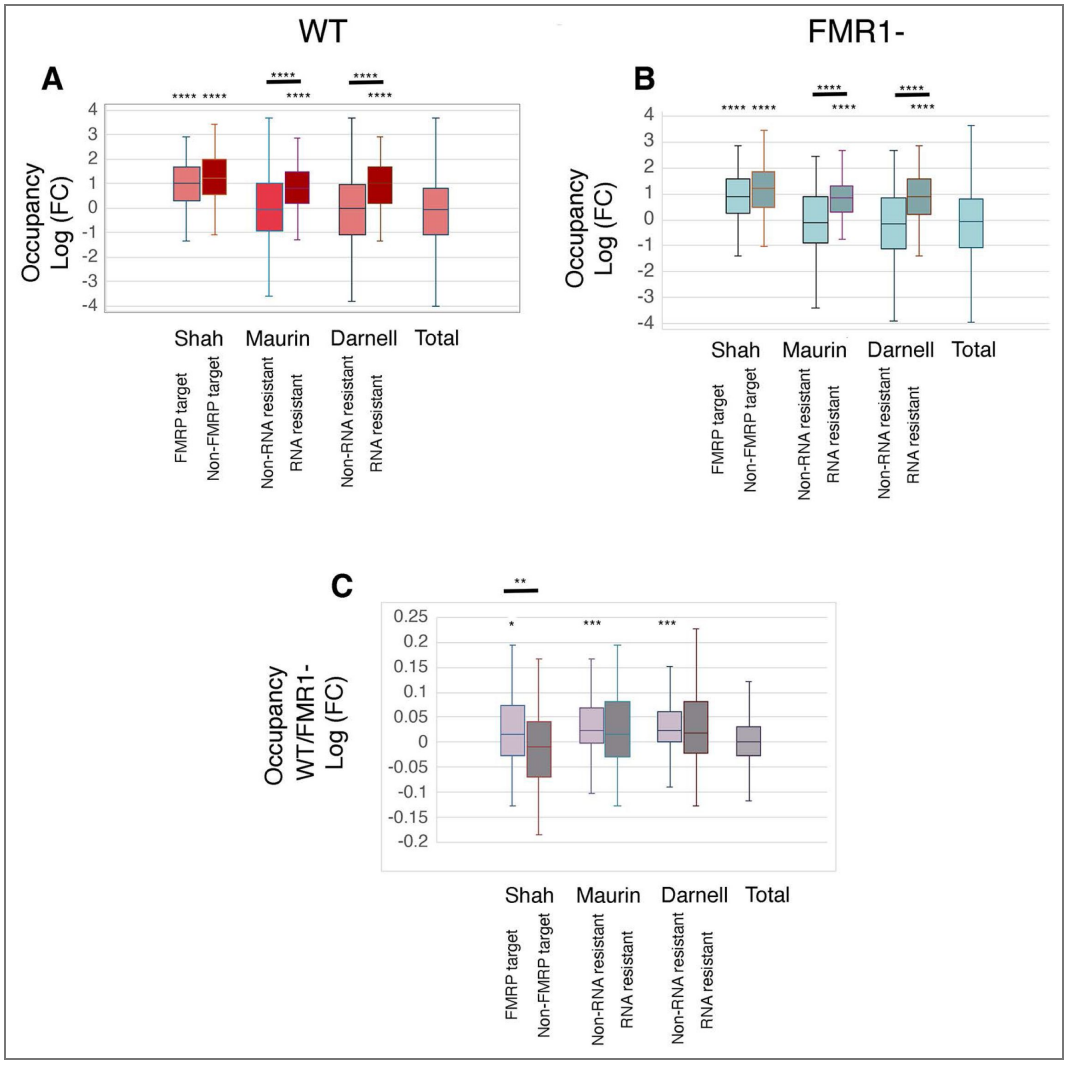

Supplemental Figure 7-1. Occupancy analysis with Subsets of FMRP Targets.and RNAs resistant to Run-Off.

The mRNAs found to be resistant to ribosome run-off (Shah et al, 2020) were divided into two sets consisting of mRNAs that are also FMRP targets (identified in Maurin et al, 2018 or Darnell et al., 2011) or not. The FMRP targets were divided into two sets consisting of mRNAs identified as one of the 200 most abundant mRNAs resistant to run-ff (Shah et al, 2020) or not. Box and Whisker plots are shown with line for mean. Different from the total RNA group using two-tailed Welch's t-test with Bonferroni correction for multiple T-tests. Differences between the two sets was also evaluated with a two-tailed Welch's t-test. A) Occupancy in WT pellet B) Occupancy in FMR1- pellet C) Difference in Occupancy between WT and FMR1-

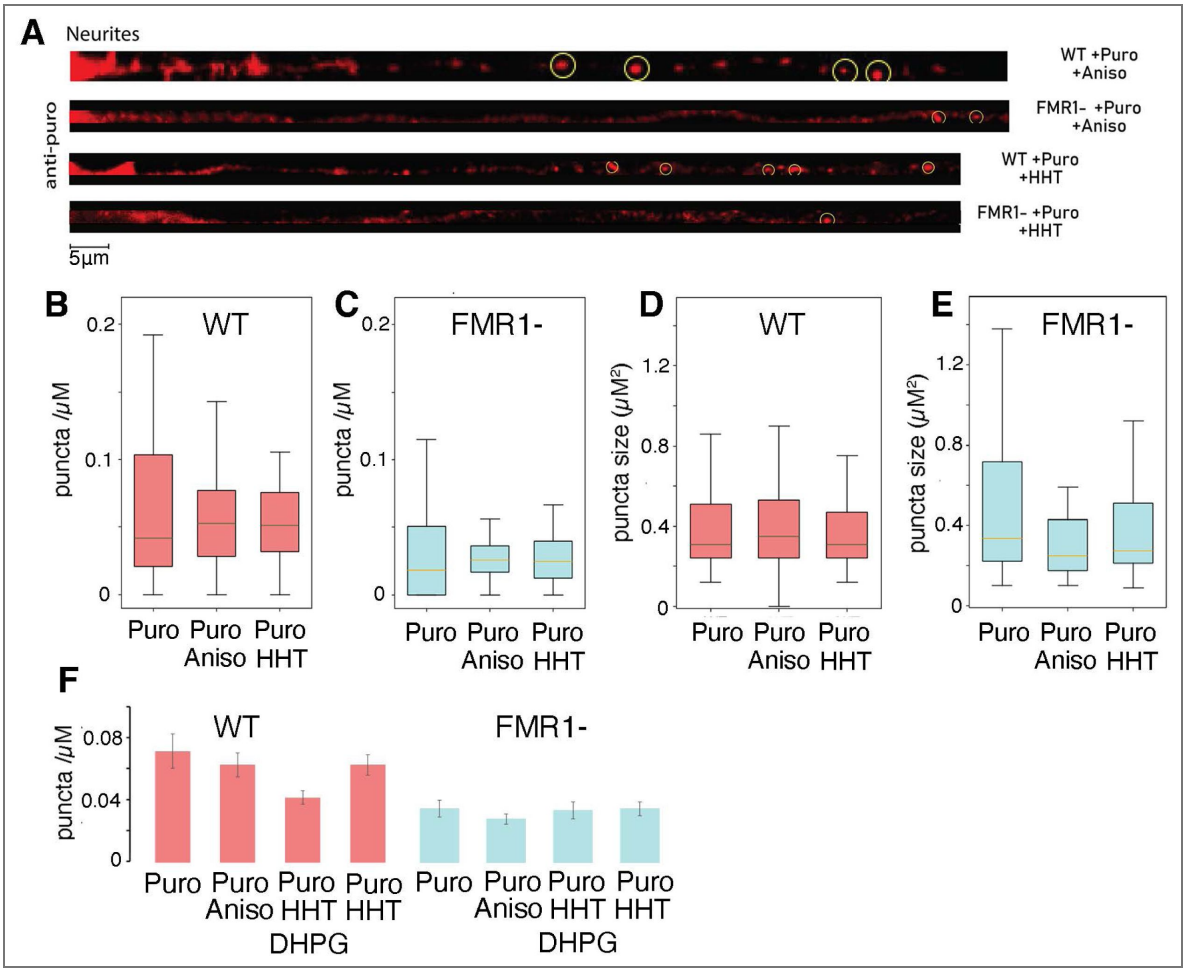

Supplementary Figure S9-1. Effect of Anisomycin and HHT on RPM of hippocampal cultures derived from WT and FMR1-mice.

A) Representative confocal images for puromycylated ribosomes treated either with puromycin and anisomycin together or pre-treated with HHT for 15 minutes before treating with puromycin. Circle denotes puromycin puncta. No visible staining was seen in the absence of puromycin. Quantification of RPM puncta density of puncta>50 microns from the cell body compared to WT (see Fig. 9) shown as box and whisker plits. There is no effect of adding anisomycin with puromycin or preincubation with HHT on the puncta density (B,D) or puncta size (C, E) in WT (B,C) or FMR1- (D,E). WT numbers are the same as Figure 9. Numbers are neurites/cultures. Puncta Density WT (42/5); WT anisomycin (A) (27/4); WT homoharringtonin (H) (36/5), FMR1- (41/4), FMR1-KO anisomycin (A) (23/3), FMRP homoharringtonin (45,5). One way ANOVA showed no significance for density or size (P>0.05). F) For clarity the data is also presented as mean +/- S.D.

	80S Class 1 (AP & PE tRNA*)	80S Class 2 (PP tRNA*)
Data Collection		
Microscope	Titan Krios	
Detector	Gatan BioQuantum LS K3	
Nominal Magnification	81,000x	
Voltage (kV)	300	
Total exposure ($e^-/Å^2$)	40	
Number of frames	30	
Defocus range (μm)	-1.25 to -2.75	
Calibrated physical pixel size (Å/px)	1.09	
Reconstruction and Refinement		
Particle number	698,894	141,803
Resolution (Å)	Consensus map (CM): 80S (2.7Å) Multi-body refinement (MBR): 40S (3.3Å) & 60S (2.7 Å)	CM: 80S (3.2Å) MBR: 40S (4.5Å) & 60S (3.2 Å)
Data Deposition		
EMDB code	EMDB-76370	EMDB- 76379

* A/P tRNA: Aminoacyl / Peptidyl transfer RNA; P/P tRNA: Peptidyl / Peptidyl transfer RNA.

Supplementary Table S4-1. Data acquisition, reconstruction and refinement parameters and data deposition codes for the cryo-EM dataset.

Additional files

Extended Data Table S3-1 List of Genes with high ratios of long reads/short reads in WT Pellet RPFs.

Extended Data Table S5-1 RNA-Seq and RKPM for all samples for all genes. Occupancy and Enrichment calculations for WT and FMR1- samples.

Extended Data Table S5-2 DEG analyses comparing WT and FMR1-.

Extended Data Table S5-3 GO analysis of WT and FMR1-.

Extended Data Table S5-4 GSEA analysis of differences between WT and FMR1- including Percentage of mRNAs matched that are FMRP targets.

Extended Data Table S6-1 Abundance, Occupancy and Enrichment for WT and FMR1- samples matching the Shah, Maurin and Darnell Lists and subsets of these lists.

Extended Data Table S7-1 Abundance, Occupancy and Enrichment comparisons of the ratio between WT and FMR1- for mRNAs matching the Shah, Maurin and Darnell Lists and subsets of these lists.

Extended Data Table S8-1 List of all Peaks as well as Motif counts.

Extended Data Table S8-2 Amino acid enrichment of Peaks.

Additional information

Funding

Funder	Grant reference number	Author
Azrieli Foundation (azrielifdn)	RNA and the Brain	Joaquin Ortega Wayne S Sossin
Canadian Institutes of Health Research (CIHR)	374967	Wayne S Sossin

Author ORCID iDs

Nahum Sonenberg: https://orcid.org/0000-0002-4707-8759
Joaquin Ortega: https://orcid.org/0000-0002-9423-3344
Wayne S Sossin: https://orcid.org/0000-0003-1927-9315

References

1. **Anadolu MN,** Sossin WS (2020) Focusing on mRNA granules and stalled polysomes amidst diverse mechanisms underlying mRNA transport, mRNA storage and local translation. In: Sossin W (Ed). *Oxford Handbook of Neuronal Protein Synthesis* Oxford Press. https://doi.org/10.1093/oxfordhb/9780190686307.013.20

2. **Anadolu MN,** Sun J, Li JT, Graber TE, Ortega J, Sossin WS (2024) Puromycin reveals a distinct conformation of neuronal ribosomes. *Proc Natl Acad Sci U S A* **121**:e2306993121 https://doi.org/10.1073/pnas.2306993121 | PubMed

3. **Anadolu MN,** Sun J, Kailasam S, Chalkiadaki K, Krimbacher K, Li JT, Markova T, Jafarnejad SM, Lefebvre F, Ortega J, *et al.* (2023) Ribosomes in RNA Granules Are Stalled on mRNA Sequences That Are Consensus Sites for FMRP Association. *J Neurosci* **43**:2440-2459 https://doi.org/10.1523/jneurosci.1002-22.2023 | PubMed

4. **Anderson BR,** Chopra P, Suhl JA, Warren ST, Bassell GJ (2016) Identification of consensus binding sites clarifies FMRP binding determinants. *Nucleic Acids Res* **44**:6649-6659 https://doi.org/10.1093/nar/gkw593 | PubMed

5. **Ascano M,** Mukherjee N, Bandaru P, Miller JB, Nusbaum JD, Corcoran DL, Langlois C, Munschauer M, Dewell S, Hafner M, *et al.* (2012) FMRP targets distinct mRNA sequence elements to regulate protein expression. *Nature* **492**:382-386 https://doi.org/10.1038/nature11737 | PubMed

6. **Aschrafi A,** Cunningham BA, Edelman GM, Vanderklish PW (2005) The fragile X mental retardation protein and group I metabotropic glutamate receptors regulate levels of mRNA granules in brain. *Proc Natl Acad Sci U S A* **102**:2180-2185 https://doi.org/10.1073/pnas.0409803102 | PubMed

7. **Bagni C,** Zukin RS (2019) A Synaptic Perspective of Fragile X Syndrome and Autism Spectrum Disorders. *Neuron* **101**:1070-1088 https://doi.org/10.1016/j.neuron.2019.02.041 | PubMed

8. **Bailey TL,** Johnson J, Grant CE, Noble WS (2015) The MEME Suite. *Nucleic Acids Res* **43**:W39-49 https://doi.org/10.1093/nar/gkv416 | PubMed

9. **Bandeira F,** Lent R, Herculano-Houzel S (2009) Changing numbers of neuronal and non-neuronal cells underlie postnatal brain growth in the rat. *Proc Natl Acad Sci U S A* **106**:14108-14113 https://doi.org/10.1073/pnas.0804650106 | PubMed

10. **Batish M,** van den Bogaard P, Kramer FR, Tyagi S (2012) Neuronal mRNAs travel singly into dendrites. *Proc Natl Acad Sci U S A* **109**:4645-4650 https://doi.org/10.1073/pnas.1111226109 | PubMed

11. **Bepler T,** Morin A, Rapp M, Brasch J, Shapiro L, Noble AJ, Berger B (2019) Positive-unlabeled convolutional neural networks for particle picking in cryo-electron micrographs. *Nat Methods* **16**:1153-1160 https://doi.org/10.1038/s41592-019-0575-8 | PubMed

12. **Carter SD,** et al. (2020) Ribosome-associated vesicles: A dynamic subcompartment of the endoplasmic reticulum in secretory cells. *Sci Adv* **6**:eaay9572 https://doi.org/10.1126/sciadv.aay9572 | PubMed

13. **Chen S,** McMullan G, Faruqi AR, Murshudov GN, Short JM, Scheres SH, Henderson R (2013) High-resolution noise substitution to measure overfitting and validate resolution in 3D structure determination by single particle electron cryomicroscopy. *Ultramicroscopy* **135**:24-35 https://doi.org/10.1016/j.ultramic.2013.06.004 | PubMed

14. **Darnell JC,** Mostovetsky O, Darnell RB (2005) FMRP RNA targets: identification and validation. *Genes Brain Behav* **4**:341-349 https://doi.org/10.1111/j.1601-183x.2005.00144.x | PubMed

15. **Darnell JC,** Van Driesche SJ, Zhang C, Hung KY, Mele A, Fraser CE, Stone EF, Chen C, Fak JJ, Chi SW, *et al.* (2011) FMRP stalls ribosomal translocation on mRNAs linked to synaptic function and autism. *Cell* **146**:247-261 https://doi.org/10.1016/j.cell.2011.06.013 | PubMed

16. **David A,** Bennink JR, Yewdell JW (2013) Emetine optimally facilitates nascent chain puromycylation and potentiates the ribopuromycylation method (RPM) applied to inert cells. *Histochem Cell Biol* **139**:501-504 https://doi.org/10.1007/s00418-012-1063-8 | PubMed

17. **Debanne D,** Campanac E, Bialowas A, Carlier E, Alcaraz G (2011) Axon physiology. *Physiol Rev* **91**:555-602 https://doi.org/10.1152/physrev.00048.2009 | PubMed

18. **Deng PY,** Klyachko VA (2021) Channelopathies in fragile X syndrome. *Nat Rev Neurosci* **22**:275-289 https://doi.org/10.1038/s41583-021-00445-9 | PubMed

19. **Duchaine T,** Wang HJ, Luo M, Steinberg SV, Nabi IR, DesGroseillers L (2000) A novel murine Staufen isoform modulates the RNA content of Staufen complexes. *Mol Cell Biol* **20**:5592-5601 https://doi.org/10.1128/mcb.20.15.5592-5601.2000 | PubMed

20. **El Fatimy R,** Davidovic L, Tremblay S, Jaglin X, Dury A, Robert C, De Koninck P, Khandjian EW (2016) Tracking the Fragile X Mental Retardation Protein in a Highly Ordered Neuronal RiboNucleoParticles Population: A Link between Stalled Polyribosomes and RNA Granules. *PLoS Genet* **12**:e1006192 https://doi.org/10.1371/journal.pgen.1006192 | PubMed

21. **Elvira G,** Wasiak S, Blandford V, Tong XK, Serrano A, Fan X, del Rayo Sanchez-Carbente M, Servant F, Bell AW, Boismenu D, *et al.* (2006) Characterization of an RNA granule from developing brain. *Molecular & cellular proteomics* **5**:635-651 https://doi.org/10.1074/mcp.m500255-mcp200 | PubMed

22. **Enam SU,** Zinshteyn B, Goldman DH, Cassani M, Livingston NM, Seydoux G, Green R (2020) Puromycin reactivity does not accurately localize translation at the subcellular level. *eLife* **9** https://doi.org/10.7554/elife.60303 | PubMed

23. **Fernandopulle MS,** Lippincott-Schwartz J, Ward ME (2021) RNA transport and local translation in neurodevelopmental and neurodegenerative disease. *Nat Neurosci* **24**:622-632 https://doi.org/10.1038/s41593-020-00785-2 | PubMed

24. **Gao Y,** Tatavarty V, Korza G, Levin MK, Carson JH (2008) Multiplexed dendritic targeting of alpha calcium calmodulin-dependent protein kinase II, neurogranin, and activity-regulated cytoskeleton-associated protein RNAs by the A2 pathway. *Mol Biol Cell* **19**:2311-2327 https://doi.org/10.1091/mbc.e07-09-0914 | PubMed

25. **Garreau de Loubresse N,** Prokhorova I, Holtkamp W, Rodnina MV, Yusupova G, Yusupov M (2014) Structural basis for the inhibition of the eukaryotic ribosome. *Nature* **513**:517-522 https://doi.org/10.1038/nature13737 | PubMed

26. **Graber TE,** Hebert-Seropian S, Khoutorsky A, David A, Yewdell JW, Lacaille JC, Sossin WS (2013) Reactivation of stalled polyribosomes in synaptic plasticity. *Proc Natl Acad Sci U S A* **110**:16205-16210 https://doi.org/10.1073/pnas.1307747110 | PubMed

27. **Graber TE,** Freemantle E, Anadolu MN, Hebert-Seropian S, MacAdam RL, Shin U, Hoang HD, Alain T, Lacaille JC, Sossin WS (2017) UPF1 Governs Synaptic Plasticity through Association with a STAU2 RNA Granule. *J Neurosci* **37**:9116-9131 https://doi.org/10.1523/jneurosci.0088-17.2017 | PubMed

28. **Hansen JL,** Moore PB, Steitz TA (2003) Structures of five antibiotics bound at the peptidyl transferase center of the large ribosomal subunit. *J Mol Biol* **330**:1061-1075 https://doi.org/10.1016/s0022-2836(03)00668-5 | PubMed

29. **Henderson R,** et al. (2012) Outcome of the first electron microscopy validation task force meeting. *Structure* **20**:205-214 https://doi.org/10.1016/j.str.2011.12.014 | PubMed

30. **Heraud-Farlow JE,** Kiebler MA (2014) The multifunctional Staufen proteins: conserved roles from neurogenesis to synaptic plasticity. *Trends Neurosci* **37**:470-479 https://doi.org/10.1016/j.tins.2014.05.009 | PubMed

31. **Hobson BD,** Kong L, Hartwick EW, Gonzalez RL, Sims PA (2020) Elongation inhibitors do not prevent the release of puromycylated nascent polypeptide chains from ribosomes. *eLife* **9** https://doi.org/10.7554/elife.60048 | PubMed

32. **Holt CE,** Martin KC, Schuman EM (2019) Local translation in neurons: visualization and function. *Nat Struct Mol Biol* **26**:557-566 https://doi.org/10.1038/s41594-019-0263-5 | PubMed

33. **Hou L,** Antion MD, Hu D, Spencer CM, Paylor R, Klann E (2006) Dynamic translational and proteasomal regulation of fragile X mental retardation protein controls mGluR-dependent long-term depression. *Neuron* **51**:441-454 https://doi.org/10.1016/j.neuron.2006.07.005 | PubMed

34. **Huber KM,** Gallagher SM, Warren ST, Bear MF (2002) Altered synaptic plasticity in a mouse model of fragile X mental retardation. *Proc Natl Acad Sci U S A* **99**:7746-7750 https://doi.org/10.1073/pnas.122205699 | PubMed

35. **Huttelmaier S,** Zenklusen D, Lederer M, Dictenberg J, Lorenz M, Meng X, Bassell GJ, Condeelis J, Singer RH (2005) Spatial regulation of beta-actin translation by Src-dependent phosphorylation of ZBP1. *Nature* **438**:512-515 https://doi.org/10.1038/nature04115 | PubMed

36. **Ingolia NT** (2014) Ribosome profiling: new views of translation, from single codons to genome scale. *Nat Rev Genet* **15**:205-213 https://doi.org/10.1038/nrg3645 | PubMed

37. **Ishizuka N,** Cowan WM, Amaral DG (1995) A quantitative analysis of the dendritic organization of pyramidal cells in the rat hippocampus. *J Comp Neurol* **362**:17-45 https://doi.org/10.1002/cne.903620103 | PubMed

38. **Kanai Y,** Dohmae N, Hirokawa N (2004) Kinesin transports RNA: isolation and characterization of an RNA-transporting granule. *Neuron* **43**:513-525 https://doi.org/10.1016/j.neuron.2004.07.022 | PubMed

39. **Khandjian EW,** Huot ME, Tremblay S, Davidovic L, Mazroui R, Bardoni B (2004) Biochemical evidence for the association of fragile X mental retardation protein with brain polyribosomal ribonucleoparticles. *Proc Natl Acad Sci U S A* **101**:13357-13362 https://doi.org/10.1073/pnas.0405398101 | PubMed

40. **Khayachi A,** Gwizdek C, Poupon G, Alcor D, Chafai M, Casse F, Maurin T, Prieto M, Folci A, De Graeve F, *et al.* (2018) Sumoylation regulates FMRP-mediated dendritic spine elimination and maturation. *Nat Commun* **9**:757 https://doi.org/10.1038/s41467-018-03222-y | PubMed

41. **Kiebler MA,** Bassell GJ (2006) Neuronal RNA Granules: Movers and Makers. *Neuron* **51**:685-690 https://doi.org/10.1016/j.neuron.2006.08.021 | PubMed

42. **Kipper K,** Mansour A, Pulk A (2022) Neuronal RNA granules are ribosome complexes stalled at the pre-translocation state. *J Mol Biol* **434**:167801 https://doi.org/10.1016/j.jmb.2022.167801 | PubMed

43. **Krichevsky AM,** Kosik KS (2001) Neuronal RNA granules: a link between RNA localization and stimulation-dependent translation. *Neuron* **32**:683-696 https://doi.org/10.1016/s0896-6273(01)00508-6 | PubMed

44. **Kurosaki T,** Mitsutomi S, Hewko A, Akimitsu N, Maquat LE (2022) Integrative omics indicate FMRP sequesters mRNA from translation and deadenylation in human neuronal cells. *Mol Cell* **82**:4564-4581. https://doi.org/10.1016/j.molcel.2022.10.018 | PubMed

45. **Langille JJ,** Ginzberg K, Sossin WS (2019) Polysomes identified by live imaging of nascent peptides are stalled in hippocampal and cortical neurites. *Learn Mem* **26**:351-362 https://doi.org/10.1101/lm.049965.119 | PubMed

46. **Lo J,** Gifford LB, Vaeth KF, Baldwin A, Bhardwaj G, Goo CEA, Mukherjee N, Russ HA, Moore JK, Taliaferro JM (2025) The RNA-binding protein HNRNPA2B1 regulates neurite RNA abundance and motor-dependent cargo transport. *Mol Biol Cell* **36**:ar152 https://doi.org/10.1091/mbc.e25-08-0383 | PubMed

47. **Martin-Solana E,** et al. (2024) Ribosome-Associated Vesicles promote activity-dependent local translation. *bioRxiv* https://doi.org/10.1101/2024.06.07.598007 | PubMed

48. **Maurin T,** Lebrigand K, Castagnola S, Paquet A, Jarjat M, Popa A, Grossi M, Rage F, Bardoni B (2018) HITS-CLIP in various brain areas reveals new targets and new modalities of RNA binding by fragile X mental retardation protein. *Nucleic Acids Res* **46**:6344-6355 https://doi.org/10.1093/nar/gky267 | PubMed

49. **McGlincy NJ,** Ingolia NT (2017) Transcriptome-wide measurement of translation by ribosome profiling. *Methods* **126**:112-129 https://doi.org/10.1016/j.ymeth.2017.05.028 | PubMed

50. **Niere F,** Wilkerson JR, Huber KM (2012) Evidence for a fragile X mental retardation protein-mediated translational switch in metabotropic glutamate receptor-triggered Arc translation and long-term depression. *J Neurosci* **32**:5924-5936 https://doi.org/10.1523/jneurosci.4650-11.2012 | PubMed

51. **Nosyreva ED,** Huber KM (2006) Metabotropic receptor-dependent long-term depression persists in the absence of protein synthesis in the mouse model of fragile X syndrome. *J Neurophysiol* **95**:3291-3295 https://doi.org/10.1152/jn.01316.2005 | PubMed

52. **Ntoulas G,** Brakatselos C, Nakas G, Asprogerakas MZ, Delis F, Leontiadis LJ, Trompoukis G, Papatheodoropoulos C, Gkikas D, Valakos D, *et al.* (2024) Multi-level profiling of the Fmr1 KO rat unveils altered behavioral traits along with aberrant glutamatergic function. *Transl Psychiatry* **14**:104 https://doi.org/10.1038/s41398-024-02815-0 | PubMed

53. **Pettersen EF,** Goddard TD, Huang CC, Couch GS, Greenblatt DM, Meng EC, Ferrin TE (2004) UCSF Chimera--a visualization system for exploratory research and analysis. *J Comput Chem* **25**:1605-1612 https://doi.org/10.1002/jcc.20084 | PubMed

54. **Pettersen EF,** Goddard TD, Huang CC, Meng EC, Couch GS, Croll TI, Morris JH, Ferrin TE (2021) UCSF ChimeraX: Structure visualization for researchers, educators, and developers. *Protein Sci* **30**:70-82 https://doi.org/10.1002/pro.3943 | PubMed

55. **Punjani A,** Rubinstein JL, Fleet DJ, Brubaker MA (2017) cryoSPARC: algorithms for rapid unsupervised cryo-EM structure determination. *Nat Methods* **14**:290-296 https://doi.org/10.1038/nmeth.4169 | PubMed

56. **Qin M,** Kang J, Burlin TV, Jiang C, Smith CB (2005) Postadolescent changes in regional cerebral protein synthesis: an in vivo study in the FMR1 null mouse. *J Neurosci* **25**:5087-5095 https://doi.org/10.1523/jneurosci.0093-05.2005 | PubMed

57. **Richter JD,** Zhao X (2021) The molecular biology of FMRP: new insights into fragile X syndrome. *Nat Rev Neurosci* **22**:209-222 https://doi.org/10.1038/s41583-021-00432-0 | PubMed

58. **Richter JD,** Bassell GJ, Klann E (2015) Dysregulation and restoration of translational homeostasis in fragile X syndrome. *Nat Rev Neurosci* **16**:595-605 https://doi.org/10.1038/nrn4001 | PubMed

59. **Santini E,** Klann E (2014) Reciprocal signaling between translational control pathways and synaptic proteins in autism spectrum disorders. *Sci Signal* **7**:re10 https://doi.org/10.1126/scisignal.2005832 | PubMed

60. **Sawicka K,** Hale CR, Park CY, Fak JJ, Gresack JE, Van Driesche SJ, Kang JJ, Darnell JC, Darnell RB (2019) FMRP has a cell-type-specific role in CA1 pyramidal neurons to regulate autism-related transcripts and circadian memory. *eLife* **8** https://doi.org/10.7554/elife.46919 | PubMed

61. **Schorb M,** Haberbosch I, Hagen WJH, Schwab Y, Mastronarde DN (2019) Software tools for automated transmission electron microscopy. *Nat Methods* **16**:471-477 https://doi.org/10.1038/s41592-019-0396-9 | PubMed

62. **Shah S,** Molinaro G, Liu B, Wang R, Huber KM, Richter JD (2020) FMRP Control of Ribosome Translocation Promotes Chromatin Modifications and Alternative Splicing of Neuronal Genes Linked to Autism. *Cell Rep* **30**:4459-4472. https://doi.org/10.1016/j.celrep.2020.02.076 | PubMed

63. **Sossin WS,** DesGroseillers L (2006) Intracellular trafficking of RNA in neurons. *Traffic* **7**:1581-1589 https://doi.org/10.1111/j.1600-0854.2006.00500.x | PubMed

64. **Sun J,** Drever L, Ortega J, Sossin WS (2025) Translation stalling in neurons: a critical mechanism for timely protein delivery to distal cellular processes. *Biochem Soc Trans* **53**:1-13 https://doi.org/10.1042/bst20253066 | PubMed

65. **Tang SJ,** Meulemans D, Vazquez L, Colaco N, Schuman E (2001) A role for a rat homolog of staufen in the transport of RNA to neuronal dendrites. *Neuron* **32**:463-475 https://doi.org/10.1016/s0896-6273(01)00493-7 | PubMed

66. **Thomson SR,** Seo SS, Barnes SA, Louros SR, Muscas M, Dando O, Kirby C, Wyllie DJA, Hardingham GE, Kind PC, *et al.* (2017) Cell-Type-Specific Translation Profiling Reveals a Novel Strategy for Treating Fragile X Syndrome. *Neuron* **95**:550-563. https://doi.org/10.1016/j.neuron.2017.07.013 | PubMed

67. **Tremblay BJ** (2024) universalmotif: An R package for biological motif analysis. *Journal of Open Source Software* **9**:7012 https://doi.org/10.5281/zenodo.13341140

68. **Udagawa T,** Farny NG, Jakovcevski M, Kaphzan H, Alarcon JM, Anilkumar S, Ivshina M, Hurt JA, Nagaoka K, Nalavadi VC, *et al.* (2013) Genetic and acute CPEB1 depletion ameliorate fragile X pathophysiology. *Nat Med* **19**:1473-1477 https://doi.org/10.1038/nm.3353 | PubMed

69. **Wong HH,** Watt AJ, Sjostrom PJ (2024) Synapse-specific burst coding sustained by local axonal translation. *Neuron* **112**:264-276. https://doi.org/10.1016/j.neuron.2023.10.011 | PubMed

70. **Wu T,** Hu E, Xu S, Chen M, Guo P, Dai Z, Feng T, Zhou L, Tang W, Zhan L, *et al.* (2021) clusterProfiler 4.0: A universal enrichment tool for interpreting omics data. *Innovation (Camb)* **2**:100141 https://doi.org/10.1016/j.xinn.2021.100141 | PubMed

71. **Yoon BC,** Zivraj KH, Holt CE (2009) Local translation and mRNA trafficking in axon pathfinding. *Results Probl Cell Differ* **48**:269-288 https://doi.org/10.1007/400_2009_5 | PubMed

72. **Yu G** (2024) Thirteen years of clusterProfiler. *Innovation (Camb)* **5**:100722 https://doi.org/10.1016/j.xinn.2024.100722 | PubMed

73. **Yu TW,** Berry-Kravis E (2014) Autism and fragile X syndrome. *Semin Neurol* **34**:258-265 https://doi.org/10.1055/s-0034-1386764 | PubMed

74. Zhang G, Xu Y, Wang X, Zhu Y, Wang L, Zhang W, Wang Y, Gao Y, Wu X, Cheng Y, *et al.* (2022) Dynamic FMR1 granule phase switch instructed by m6A modification contributes to maternal RNA decay. *Nat Commun* **13**:859 https://doi.org/10.1038/s41467-022-28547-7 | PubMed

Peer reviews

Reviewer #1 (Public review):

Summary:

Authors have investigated the role of FMRP in the formation and function of RNA granules in mouse brain/cultured hippocampal neurons. Most of their results indicate that FMRP does not have a role in the formation or function of RNA granules with specific mRNAs but may have some role in distal RNA granules in neurons and their response to synaptic stimulation. This is an important work (though the results are mostly negative) in understanding the composition and function of neuronal RNA granules. the last part of the work in cultured neurons is disjointed from the rest of the manuscript and the results are neither convincing nor provide any mechanistic insight.

Strengths:

(1) The study is quite thorough, the methods and analysis used are robust and the conclusion and interpretation are diligent.

(2) The comparative study of Rat and Mouse RNA granules is very helpful for future studies

(3) The conclusion that the absence of FMRP does not affect the RNA granule composition and many of its properties in the system the authors have chosen to study is well supported by the results

(4) The difference in the response to DHPG stimulation concerning RNA granules described here is very interesting and could provide a basis for further studies though it has some serious technical issues (see below)

Weaknesses:

(1) The system used for the study (P5 mouse brain or DIV 8-10 cultured neuron) is surprising as the majority of defects in the absence of FMRP are reported in later stages (P30+ brain and DIV 14+ neurons). It is important to test if the conclusions drawn here hold good at different developmental stages.

(2) The term 'distal granules' is very vague. Since there is no structural or biochemical characterization of these granules it is difficult to understand how they are different from the proximal granules and why FMRP has an effect only on these granules.

(3) Since the manuscript does not find any effect of FMRP on neuronal RNA granules, it does not provide any new molecular insight with respect to the function of FMRP

Comments on revised version.

The authors have answered several questions raised by the reviewers. But for me, the critical issue of using only the brain from P5 animals and relatively early DIV neurons is still not convincingly addressed. FMRP may still play a role in determining the stalled ribosomes on its target mRNAs at a later stage of development, when there is more scope for activity-mediated protein synthesis.

I agree with the authors that this work helps the molecular understanding of FMRP functions by disproving one of the long-standing hypotheses.

https://doi.org/10.7554/eLife.106692.2.sa3

Reviewer #2 (Public review):

In the present manuscript, Li et al. use biochemical fractionation of "RNA granules" from P5 wildtype and FMR1 knock-out mouse brains to analyze their protein/RNA content, determine a single particle cryo-EM structure of contained ribosomes, and perform ribo-seq analysis of ribosome-protected RNA fragments (RPFs). The authors conclude from these that neither the composition of the ribosome granules, nor the state of their contained ribosomes, nor the mRNA positions with high ribosome occupancy change significantly. Besides minor changes in mRNA occupancy, the one change the authors identified is a decrease in puromycylated punctae in distal neurites of cultured primary neurons of the same mice, and their enhanced resistance to different pharmacological treatments. These results directly build on their earlier work (Anadolu et al., 2023) using analogous preparations of rat brains; the authors now perform a very similar study using WT and FMR1-KO mouse brains. This is an important topic, aiming to identify the molecular underpinnings of the FMRP protein, which is the basis of a major neurological disease. Unfortunately, several limitations of this study prevent it from being more convincing in its present form.

In order to improve this study, our main suggestions are as follows:

(1) The authors equate their biochemically purified "RG" fraction with their imaging-based detection of puromycin-positive punctae. They claim essentially no differences in RGs but detect differences in the latter (mostly their abundance and sensitivity to DHPG/HHT/Aniso). In the discussion the authors acknowledge the inconsistency between these two modalities: "An inconsistency in our findings is the loss of distal RPM puncta coupled with an increase in the immunoreactivity for S6 in the RG." and "Thus, it may be that the RG is not simply made up of ribosomes from the large liquid-liquid phase RNA granules."

How can the authors be sure that they are in fact analysing the same entities in both modalities? A more parsimonious explanation of their results would be that, while there might be some overlap, two different entities are analyzed. Much of the main message rests on this equivalence and I believe the authors should show its validity.

(2) The authors show that increased nuclease digestion (and magnesium concentration) led to a reduction of their RPF sizes down to levels also seen by other researchers. Analyzing these now properly digested RPFs, the authors state that the CDS coverage and periodicity drastically improved, and that spurious enrichments of secretory mRNAs, which made up one of the major fractions in their previous work, are now reduced. In my opinion this would be more appropriately communicated as a correction to their previous work, not as a main Figure in another manuscript.

(3) The fold changes reported in Figure 7 (ranging between log2(-0.2) and log2(+0.25)) are all extremely small and in my opinion should not be used to derive claims such as "The loss of FMRP significantly affected the abundance and occupancy of FMRP-Clipped mRNAs in WT and FMR1-KO RG (Fig 7A, 7B), but not their enrichment between RG and RCs".

(4) Fig 8 / S8-1 - The authors show that ~2/3 of their reads stem from PCR duplicates, but that even after removing those, the majority of peaks remains unaltered. At the same time, Fig S8-1 shows the total number of peaks to be 615 compared with 1392 before duplicate removal. Can the authors comment on this discrepancy? In addition, the dataset with properly removed artefacts should be used for their main display item instead of the current Fig 8.

(5) Fig 9 / S9-1, the density of punctae in both WT and FMR1-KO actually increases after treatment of HHT or Anisomycin (Fig S9-1 B-C). Even if a large fraction would now be "resistant to run-off", there should not be an increase. While this effect is deemed not

significant, a much smaller effect in Fig 9C is deemed significant. Can the authors explain this? Given how vastly different the sample sizes are (ranging from 23 neurites in Fig S9-1 to 5,171 neurites in Fig 9), the authors should (randomly) sample to the same size and repeat their statistical analysis again to improve their credibility.

Comments on revised version.

We can see that the authors invested substantial effort to improve the manuscript and we believe it is improved.

https://doi.org/10.7554/eLife.106692.2.sa2

Reviewer #3 (Public review):

Summary:

Li et al describe a set of experiments to probe the role of FMRP in ribosome stalling and RNA granule composition. The authors are able to recapitulate findings from a previous study performed in rats (this one is in mice).

Strengths:

(1) The work addresses an important and challenging issue, investigating mechanisms that regulate stalled ribosomes that are part of stress granules, and focusing on the role of FMRP. This is a complicated problem, given the heterogeneity of the granules and the challenges related to their purification. This work is a solid attempt at addressing this issue, which is widely understudied.

(2) The interpretation of the results could be interesting, if supported by solid data. The idea that FMRP could control the formation and release of stress granules, rather than the elongation by stalled ribosomes is of high importance to the field, offering a fresh perspective into translational regulation by FMRP.

(3) The authors focused on recapitulating previous findings, published elsewhere (Anadolu et al., 2023) by the same group, but using rat tissue, rather than mouse tissue. Overall, they succeeded in doing so, demonstrating, among other findings, that stalled ribosomes are enriched in consensus mRNA motifs that are linked to FMRP. These interesting findings reinforce the role of FMRP in formation and stabilization of RNA granules. It would be nice to see extensive characterization of the mouse granules as performed in Figure 1 of Anadolu and colleagues, 2023.

(4) Some of the techniques incorporated aid in creating novel hypotheses, such as the ribopuromycilation assay and the cryo-EM of granule ribosomes.

Comments on revised version:

I am satisfied with the authors response to my comments.

https://doi.org/10.7554/eLife.106692.2.sa1

Author response:

The following is the authors' response to the original reviews.

We have addressed all the reviewers' comments through new experiments, additional analyses, or, in some cases, additional text. Below is a summary of the major changes in the manuscript.

(1) We have added a considerable amount of new characterization of the biochemical enrichment of the ribosome clusters, including EM of the ribosome clusters, UV absorbance profiles, immunoblots of additional targets, and additional replicates (new Figure 1). In summary, we provide better evidence that (i) the biochemical enrichment is working and (ii) that the loss of FMRP has no effect on this biological enrichment of ribosomal clusters.

(2) We have now reanalyzed all of the data in Figs. 5-8 using only the data after removing PCR duplicates from the RPFs. Other than the comparison between the nuclease treatments (Fig. 3), only this data is now used. Moreover, we have reanalyzed this data using suggestions from the reviewers, including providing PCA analysis (Fig S5-1), GSEA analysis (Fig 5), and normalizing for group size when comparing significance to total mRNAs, (Fig 6-7). We now also include a new analysis (Fig S7-1) to better explain how the loss of FMRP affects mainly FMRP targets defined by CLIP, but not all mRNAs resistant to run-off.

(3) We are now more conservative in our nomenclature; we use "pellet" instead of "RNA granule (RG)" and "fraction 5/6" instead of "ribosome clusters (RC)". We have added a section to the discussion about the relationship between the RNA granules measured using imaging of hippocampal neurites and the biochemical purification of ribosome clusters in the pellet, as requested by the reviewers.

(4) We have made many other minor changes to the text and analysis, which can be found in the specific response to the reviewers.

(5) One major additional requested change that was not implemented was to repeat our experiments at different time points. We have added a paragraph to the discussion outlining (i) why this was not done and (ii) the caveats of our conclusions without this data being present.

> ***Public Reviews:***
>
> ***Reviewer #1 (Public review):***
>
> *Summary:*
>
> *The authors have investigated the role of FMRP in the formation and function of RNA granules in mouse brain/cultured hippocampal neurons. Most of their results indicate that FMRP does not have a role in the formation or function of RNA granules with specific mRNAs, but may have some role in distal RNA granules in neurons and their response to synaptic stimulation. This is an important work (though the results are mostly negative) in understanding the composition and function of neuronal RNA granules. The last part of the work in cultured neurons is disjointed from the rest of the manuscript, and the results are neither convincing nor provide any mechanistic insight.*
>
> *Strengths:*
>
> *(1) The study is quite thorough, the methods and analysis used are robust, and the conclusion and interpretation are diligent.*
>
> *(2) The comparative study of Rat and Mouse RNA granules is very helpful for future studies.*
>
> *(3) The conclusion that the absence of FMRP does not affect the RNA granule composition and many of its properties in the system the authors have chosen to study is well supported by the results.*
>
> *(4) The difference in the response to DHPG stimulation concerning RNA granules described here is very interesting and could provide a basis for further studies, though it*

> *has some serious technical issues.*

Thank you for these positive comments on the paper.

> *Weaknesses:*
>
> *(1) The system used for the study (P5 mouse brain or DIV 8-10 cultured neuron) is surprising, as the majority of defects in the absence of FMRP are reported in later stages (P30+ brain and DIV 14+ neurons). It is important to test if the conclusions drawn here hold good at different developmental stages.*

Unfortunately, myelin strongly interferes with the ability to use this protocol to purify ribosome clusters in older brains (See Khandjian et al., 2004). It is possible to redo the ribopuromycylation results at later times in culture, but since we cannot compare this to a comparable time in the brain, we have chosen not to do this experiment. We acknowledge this limitation in the discussion, noting that our results are only a snapshot of development and that different results may be observed at different times.

> *(2) The term 'distal granules' is very vague. Since there is no structural or biochemical characterization of these granules, it is difficult to understand how they are different from the proximal granules and why FMRP has an effect only on these granules.*

We agree with the reviewer and have removed all references to distal granules. We clarified that we did not measure RPM puncta close to the neuron because the much stronger RPM signal made defining puncta more difficult, and thus, we cannot determine if there are differences between proximal and distal puncta.

> *(3) Since the manuscript does not find any effect of FMRP on neuronal RNA granules, it does not provide any new molecular insight with respect to the function of FMRP*

We would respectfully disagree that the study does not provide molecular insight into the function of FMRP, as disproving that FMRP is important for stalling and determining the position of stalling would remove one of the major hypotheses about the function of FMRP, and showing that a major hypothesis in the literature is unlikely to be correct, is at least to me, providing insight. Moreover, we do show an effect of the loss of FMRP on the RPM puncta that represent neuronal RNA granules containing stalled ribosomes. This also provides insight.

> ***Reviewer #2 (Public review):***
>
> *In the present manuscript, Li et al. use biochemical fractionation of "RNA granules" from P5 wildtype and FMR1 knock-out mouse brains to analyze their protein/RNA content, determine a single particle cryo-EM structure of contained ribosomes, and perform ribo-seq analysis of ribosome-protected RNA fragments (RPFs). The authors conclude from these that neither the composition of the ribosome granules, nor the state of their contained ribosomes, nor the mRNA positions with high ribosome occupancy change significantly. Besides minor changes in mRNA occupancy, the one change the authors identified is a decrease in puromycylated punctae in distal neurites of cultured primary neurons of the same mice, and their enhanced resistance to different pharmacological treatments. These results directly build on their earlier work (Anadolu et al., 2023) using analogous preparations of rat brains; the authors now perform a very similar study using WT and FMR1-KO mouse brains. This is an important topic, aiming to identify the molecular underpinnings of the FMRP protein, which is the basis of a major neurological disease. Unfortunately, several limitations of this study prevent it from being more convincing in its present form.*
>
> *In order to improve this study, our main suggestions are as follows:*

> *(1) The authors equate their biochemically purified "RG" fraction with their imaging-based detection of puromycin-positive punctae. They claim essentially no differences in RGs, but detect differences in the latter (mostly their abundance and sensitivity to DHPG/HHT/Aniso). In the discussion the authors acknowledge the inconsistency between these two modalities: "An inconsistency in our findings is the loss of distal RPM puncta coupled with an increase in the immunoreactivity for S6 in the RG." and "Thus, it may be that the RG is not simply made up of ribosomes from the large liquid-liquid phase RNA granules."*
>
> *How can the authors be sure that they are analysing the same entities in both modalities? A more parsimonious explanation of their results would be that, while there might be some overlap, two different entities are analyzed. Much of the main message rests on this equivalence, and I believe the authors should show its validity.*

Thank you for your comments. We have been more conservative in the revised paper, referring to the pellet fraction as the pellet fraction rather than the RNA granule fraction to acknowledge the possibility that these two modalities differ. However, we would respectfully disagree that our main message requires RPM-labeled RNA granules in neurites and the ribosome clusters isolated by sedimentation to be “equivalent”. We do believe they are related and added a section in the discussion on this important point.

> *(2) The authors show that increased nuclease digestion (and magnesium concentration) led to a reduction of their RPF sizes down to levels also seen by other researchers. Analyzing these now properly digested RPFs, the authors state that the CDS coverage and periodicity drastically improved, and that spurious enrichments of secretory mRNAs, which made up one of the major fractions in their previous work, are now reduced. In my opinion, this would be more appropriately communicated as a correction to their previous work, not as a main Figure in another manuscript.*

We have removed all discussion of the secretory mRNAs, as our attempts to obtain independent evidence for this finding by examining ribophorin enrichment in the pellet across different Mg^{2+} concentrations did not support this interpretation (data not shown in the paper). I understand that the change in nuclease is somewhat out of place narratively, but it is clearly relevant to this work. We would disagree with our previous work requiring a ‘correction’. We believe that the nuclease resistance of the mRNA at the entrance site is important. We reproduce our results from rats with similar nuclease treatment in mice as seen in our previous publication; thus, this work is not wrong. We have a paper in preparation that suggests the secondary structure of the mRNA at this location may be important for stalling and thus feel strongly that this result should remain in the manuscript.

> *(3) The fold changes reported in Figure 7 (ranging between log2(-0.2) and log2(+0.25)) are all extremely small and in my opinion should not be used to derive claims such as "The loss of FMRP significantly affected the abundance and occupancy of FMRP-Clipped mRNAs in WT and FMR1-KO RG (Fig 7A, 7B), but not their enrichment between RG and RCs".*

We agree that the changes are small and indeed did not appear in the DEG analysis. However, because we are analyzing a large set of mRNAs in this analysis, the results are highly significant and remain significant when using the new statistical tests suggested by the reviewer below. We now emphasize that these are small changes and remind readers that none of the individual mRNA changes were significant in the DEG analysis.

> *(4) Figure 8 / S8-1 - The authors show that ~2/3 of their reads stem from PCR duplicates, but that even after removing those, the majority of peaks remain unaltered. At the same time, Figure S8-1 shows the total number of peaks to be 615 compared with 1392 before*

> *duplicate removal. Can the authors comment on this discrepancy? In addition, the dataset with properly removed artefacts should be used for their main display item instead of the current Figure 8.*

We now use only the data after removing PCR duplicates for all the analyses except in Figure 3. The number of peaks observed is determined mainly by the threshold used, as stated in the methods “To be identified as a peak, the zenith of an abundance site for the reads must be 4x higher of the average of the total transcript.” Due the lower number of reads after the PCR duplicates fewer peaks reached this threshold.

> *(5) Figure 9 / S9-1, the density of punctae in both WT and FMR1-KO actually increases after treatment of HHT or Anisomycin (Figure S9-1 B-C). Even if a large fraction would now be "resistant to run-off", there should not be an increase. While this effect is deemed not significant, a much smaller effect in Figure 9C is deemed significant. Can the authors explain this? Given how vastly different the sample sizes are (ranging from 23 neurites in Figures S91 to 5,171 neurites in Figure 9), the authors should (randomly) sample to the same size and repeat their statistical analysis again, to improve their credibility.*

The box and whisker plots emphasize the median and not the average. We now also show the averages in Figure S9-1, which indicate a slight decrease for both HHT and anisomycin.

We apologize for the typo in the figure legend in Figure 9, 171, not 5171. We now use random sampling in Figures 6 and 7, where the sample sizes differ substantially.

> ***Reviewer #3 (Public review):***
>
> *Summary:*
>
> *Li et al describe a set of experiments to probe the role of FMRP in ribosome stalling and RNA granule composition. The authors are able to recapitulate findings from a previous study performed in rats (this one is in mice).*
>
> *Strengths:*
>
> *(1) The work addresses an important and challenging issue, investigating mechanisms that regulate stalled ribosomes that are part of stress granules, and focusing on the role of FMRP. This is a complicated problem, given the heterogeneity of the granules and the challenges related to their purification. This work is a solid attempt at addressing this issue, which is widely understudied.*
>
> *(2) The interpretation of the results could be interesting if supported by solid data. The idea that FMRP could control the formation and release of stress granules, rather than the elongation by stalled ribosomes, is of high importance to the field, offering a fresh perspective into translational regulation by FMRP.*
>
> *(3) The authors focused on recapitulating previous findings, published elsewhere (Anadolu et al., 2023) by the same group, but using rat tissue, rather than mouse tissue. Overall, they succeeded in doing so, demonstrating, among other findings, that stalled ribosomes are enriched in consensus mRNA motifs that are linked to FMRP. These interesting findings reinforce the role of FMRP in the formation and stabilization of RNA granules. It would be nice to see extensive characterization of the mouse granules as performed in Figure 1 of Anadolu et al., 2023.*
>
> *(4) Some of the techniques incorporated aid in creating novel hypotheses, such as the ribopuromycilation assay and the cryo-EM of granule ribosomes.*

Thank you for these positive comments. We have now added a more extensive characterization in Figure 1.

> *Weaknesses:*
>
> *(1) The RNA granule characterization needs to be more rigorous. Coomassie is not proper for this type of characterization, simply because protein weight says little about its nature. The enrichment of key proteins is not robust and seems not to reach significance in multiple instances, including S6 and UPF1. Furthermore, S6 is the only proxy used for ribosome quantification. Could the authors include at least 3 other ribosomal proteins (2 from the small, 2 from the large subunit)?*

We have increased N to improve the robustness of the enrichment analysis and added several additional RBPs. Along with Coomassie we now include analysis of UV absorbance and include EMs from these fractions showing the presence of 80S ribosomal clusters in the fractions we are using.

> *(2) Page 12-13 - The Gene Ontology analysis is performed incorrectly. First, one should not rank genes by their RPKM levels. It is well known that housekeeping genes, such as those related to actin dynamics, molecular transport, and translation, are highly enriched in sequencing datasets. It is usually more informative when significantly different genes are ranked by p-adjust or log2 Fold Change, then compared against a background to verify enrichment of specific processes. However, the authors found no DEGs. I would suggest the removal of this analysis and the incorporation of a gene set enrichment analysis (ranked by p-adjust). I further suggest that the authors incorporate a dimensionality reduction analysis to demonstrate that the lack of significance stems from biology and not experimental artifacts, such as poor reproducibility across biological replicates.*

Thank you for the suggestion. We now use GSEA analysis to examine differences in gene sets between WT and FMR1- mice and find some significant changes (new Fig. 5). The old analysis is still included for comparison to our earlier paper as a supplemental figure. We have now included a PCA analysis (FigS5-1) to show reproducibility across biological replicates.

> ***Recommendations for the authors:***
>
> ***Reviewer #1 (Recommendations for the authors):***
>
> *(1) RNA sequencing comparison between WT and FMR1 KO mice should be carried out at a later developmental stage, which may provide a better difference between these two groups*

There are a number of studies that have already done this analysis and in specific brain regions 10.1016/j.neuron.2017.07.013; 10.7554/eLife.46919; 10.3389/fnmol.2017.00340; *https://doi.org/10.1016/j.neuron.2023.06.009*. The main goal of our RNA-seq was to standardize for the RPF studies, not to identify differences in RNA-seq between WT and FMRP. In the response to public review point 1 we explain why we do not look at later developmental timepoints.

> *(2) The same is true in characterizing the effect of FMRP on the RNA granules.*

See response to public review point 1, which addresses this point.

> *(3) No evidence is provided for the effectiveness of DHPG stimulation in DIV8-10 neurons; this is needed for justification using neurons at this stage.*

We have previously shown that DHPG stimulation in these neurons at this developmental time from cultures made from rat brain is sufficient to decrease the number of RPM puncta and to induce an increase in the synthesis of proteins in an initiation resistant manner (Graber et al, 2013; Graber et al, 2017). This is now more clearly stated in the manuscript.

Moreover, here we replicate the result of DHPG in WT mice at reducing the number of RPM puncta.

> *(4) In Figure 9 B, it is not clear whether the neurites indicated are axons or dendrites. Since neurons are still in the early stages of dendritogenesis/synaptogenesis, it is important to make that distinction.*

We have previously characterized RNA granules in axons and dendrites in hippocampal cultures from rats at this time (Miller et al, 2009, MCN 40:485-495)) and they are similar. While it is likely that the vast majority of the neurites at this time are dendrites, since we did not use markers, we conservatively just use the term neurites.

> *(5) In Figure 1 (and elsewhere), fraction 5/6 is used as a polysome or RNA cluster. The authors have not provided a UV absorption profile and only have s6 as evidence to say this polysome. In the Coomassie gel, this fraction is any different than fractions 7/7 or 9/10; what is the justification for using this fraction?*

The main justification for these fractions is to be consistent with our previous paper (Anadolu et al, 2023) and the Khandian study comparing polysomes to pellet using the same fractionation protocol (El-Fatimy et al, 2016). We now provide a UV absorption profile (Fig. 1C) and EM pictures (Fig. 1D) to show the ribosome clusters in this fraction. We do not believe our results would be fundamentally different from those obtained if we had used other heavy fractions.

> *Minor comments*
>
> *(1) The font size very small in the figures, please increase it.*

We have worked hard to increase the font size in all the figures.

> *(2) In the result section for Figure 3B - it is written 'majority of these mRNA are non-coding mRNA' - this doesn't make sense.*

Corrected

> ***Reviewer #2 (Recommendations for the authors):***
>
> *(1) There are lots of mistakes (e.g. word omissions or duplications, grammatical errors) throughout the text, too many to list here.*

We have carefully edited the text to try to minimize these mistakes.

> *(2) In many positions related to their improved nuclease digestion protocol, samples are labelled "M ...", which apparently stands for "high magnesium and high nuclease treatment group". I would suggest switching to something more intuitive, such as "... (improved digestion)".*

We have removed most of the comparisons between these samples. What remains (Figure 3), we just use Low Nuclease when we refer to the sample with low Magnesium and low nuclease.

> *(3) Figure 1,3 - It would be tremendously illuminating to see a polysome trace (UV260 absorbance) in addition to Coomassie-stained SDS-PAGE to underscore the interpretation of the different fractions by the authors. As it stands, there is no way of telling whether there are any polysomes present at all. This can also be done by hand using a UV absorption reader if no built-in device is available to the authors.*

We have now done this (Fig. 1C) and also provided EM of this fraction to show the presence of ribosomes in this fraction.

> *(4) I don't understand why the authors switched from calling fraction 5/6 the "polysome fraction" in their previous work to calling it "ribosome cluster fraction" in this work. The argument given "[...] due to its structural similarity to ribosomes in RNA Granules (Anadolu et al., 2023), we conservatively call this the ribosome cluster fraction (RC)." does not instill confidence that these two fractions are indeed distinct.*

We agree with the reviewer and regret this decision. We now call the pellet, the pellet and Fraction 5/6, fraction 5/6.

> *(5) Figure 1C - There are clear scanning or compression artefacts in the blot images (most prominently in the eEF2 lanes) that should be corrected.*

We have replaced all images in Figure 1 and have increased the N of this experiment considerably.

> *(6) Figure 1C - The authors claim that WT mouse RG is enriched in FMRP compared to RC or starter fraction, but there is also a lot more protein loaded in the RG (especially when compared to RC). It is also hard to believe from the Coomassie staining that despite the much stronger presence of low MW bands (which is where ribosomal proteins migrate) in fraction 5/6, the s6 western blot signal is actually comparable between RC and RG. Can the authors please provide more detail on the loading of these fractions and supply quantification of FMRP in all three fractions, normalized by total protein? This might also be the source of their discrepancy, stating that contrary to their expectation, ribosomes (as measured by s6 signal / s6 signal in starter fraction) are actually increased in FMR1-KO brains.*

We have repeated all of these experiments and changed our method of quantification (See methods). We no longer use the starting material in our quantification. Indeed, with the additional data and change in method, we no longer see an increase in S6 in the FMR1- pellet fraction.

> *(7) Figure 1 - I believe "D-F)" should only read "D-E)" based on the axis titles, and instead "FG)" should be added before the next sentence. Instead of "Staufen" it should be specified in the Figure that "Stau2" was quantified. "Staufen (59kd)" should read "Stau2 (59 kDa)" and "anti-Staufen (52kb)" should read "anti-Stau2 (52 kDa)" and the same for all other similar instances. It is further hard to believe that e.g., "Staufen2 (59kd)" (see above) is not significantly enriched with N=5, a very low spread, and over 1.5x enrichment. The authors should double-check that the appropriate statistical test was employed.*

Figure 1 has been completely redone, and the two Staufen bands are enriched in this new analysis.

> *(8) Figure S4-2 - Most of the detail in the corresponding figure legend should be moved to the Materials and Methods section.*

Details relevant to the methods in this figure legend have been now moved to the Material and Methods section.

> *(9) Figure 4A - The displayed/segmented tRNA densities appear unusually distorted. I would recommend displaying segmented densities of the original homogeneous reconstructions, not of separated and later fused partial maps.*

Figure 4 was modified according to the suggestions of this reviewer.'

> *(10) Figure 9 C-D, S9-1 B-E - Are not all conditions also including puromycin as in B above? If so, it should be added to both the figure and the figure legend.*

The reviewer is correct and the figure and legend has been changed to reflect this.

> ***Reviewer #3 (Recommendations for the authors):***
>
> *(1) "Loss of FMRP causes Fragile X syndrome. In humans, the loss of FMRP occurs due to the expansion of a CGG repeat in the 5' untranslated region (UTR) of the gene, leading to excessive methylation and transcriptional inhibition."*
>
> *Comment: Genes don't have 5'UTR, but exons encoding 5'UTR. I suggest rephrasing this statement.*

This sentence has been rephrased.

> *(2) "Several of these functions have been implicated in Fragile X syndrome, including FMRP's regulation of miRNA repression, splicing, translation initiation, and translational elongation".*
>
> *Comment: Is this a typo? miRNA instead of mRNA?*

No, this is correct. FMRP has been implicated in the regulation of microRNAs (miRNAs) in a number of studies.

> *(3) "elongation rates are also increased in mouse models of FMRP".*
>
> *Comment: Mouse models of Fragile X?*

This has been corrected.

> *(4) "Parts of this work were included in the Master's thesis of the first author (Li, 2024)."*

This has been removed.

> *(5) Comment: Graphs in Figure 1 need proper y-axis labeling. What is the normalization method? What are the values presented in the y-axis?*

Figure 1 has been completely changed and the Y-axes are now clear in this new version.

> *(6) "Thus, by looking at the percentage of puromycylation present in the presence of anisomycin, we can estimate the number of ribosomes in this state. "*
>
> *Comment: Are the authors really estimating the number of ribosomes in a resistant state? One could argue that they are collecting populational information regarding resistance to anisomycin.*

We have rephrased this sentence to be more conservative about what we are measuring.

> *(7) Comment: Page 11 - Why did the authors assume magnesium would affect the conformation state of the ribosomes? What is the rationale behind increasing the [Mg2+]?*

Most preparations using ribosomes use 10 mM $MgCl_2$. However, most neuroscientists use physiological buffers that contain 2.5 mM $MgCl_2$. In bacteria, this makes a large difference, but evidence from eukaryotes is not clear. Since this is a collaboration between these two schools of thought, we decided to switch to 10 mM $MgCl_2$, since in the EM, there were some free 60S ribosomes (Anadolu et al, 2024).

> *(8) Page 11- "In other words, high Mg2+ decreased the abundance of mRNAs normally cotranslationally inserted into the ER which are unlikely to be components of*

> *transporting RNA granules containing stalled ribosomes and solidified our focus on the M protocol in the analyses below."*

We have removed this from the paper, as additional experiments aimed to solidify this interpretation failed to detect an effect on secretory mRNAs.

> *(9) Comment: The whole "abundance", "enrichment", and "occupancy" nomenclature is hard to follow.*

We have rewritten this section.

> *(10) Page 13 - "There were only 2 protein coding genes that were significantly different between the abundance of FMR1-KO and WT in protein coding genes - FMR1 and Wdfy1 (Extended Data Table 5-2). There were no significantly different genes between WT and FMR1-KO occupancy and enrichment. Thus, no difference rose to significance, given the large number of mRNAs used in this analysis."*
>
> *Comment: It seems like this is repeating the same information three times.*

This has been changed.

> *(11) Page 13 - "Similar to previous experiments with rats, the most abundant mRNAs resistant to run off were significantly abundant, occupied and enriched in both WT and FMRP RPFs (Fig 6)"*

The Shah et al dataset we use was based on the most abundant mRNAs resistant to run-off. While we agree it is not surprising that they are also abundant in the pellet we observe, this would not necessarily be true unless the pellet is actually enriched in stalled mRNAs.

> *(12) Page 14 - "These mRNAs had been identified by cross-linking FMRP with mRNA, fragmenting the mRNA, immunoprecipitating the mRNA still associated with FMRP and sequencing this mRNA."*

We shortened this description.

> *(13) Page 14 - "Interestingly, while still significant, there appeared to be a decrease in the relative abundance of these mRNAs in the FMR1-KO RG (Fig 6B)"*
>
> *Comment: It is hard to observe this decrease in the boxplots. Second, the statistical tests for the bioinformatics analyses are not the most appropriate, given the large discrepancy in the number of mRNAs present in the experimental group ("All mRNAs") and the filtered groups.*

We have redone the statistics using multiple random sampling of all the mRNAs such that the total number of mRNAs in the group was the same. This lowered the significance for some groups, but they are mostly still highly significant. This analysis has also been affected by switching to using the data from the PCR-subtracted RPFs. The changes we now observe are more evident in the whisker box plots due to this improvement in the data.

> *(14) Page 16 - "To rule out that peaks were due to amplification artifacts in the preparation of RPFs we repeated these analyses after removing PCR duplicates (Fig. S8-1; Extended Data Table S8-3) and found over 95% of the peaks identified without removing PCR duplicates were defined as a peak in at least one of the biological replicates after removing duplicates. More importantly, we found similar results with enrichment of FXS motif and enrichment of negatively charged amino acids in the FMR1-KO only, WT only and both peaks after removing PCR duplicates (Fig. S8-1; Extended Data Table S8-3)."*
>
> *Comment: It is unclear why the authors needed to include the analysis without PCR duplicate removal. This is an essential step to guarantee the robustness of ribo-seq*

> *findings. I recommend removing the whole analysis from Figure 8 from the manuscript and including only the post-duplicate removal analysis.*

As mentioned above, we completely agree with this statement and now show only this data and moreover have redone all the figures with only this data (except for Fig. 3).

> *(15) Figure 9 - I am unsure that the data is convincing enough to demonstrate reinitiation of mRNA granules induced by DHPG. I suggest a colocalization experiment with another protein well known to be localized to RNA granules, such as G3BP1. In addition, repeat the experiment with an additional group where elongation is blocked after the addition of DHPG, which presumably would prevent the reduction in the WT puncta density.*

These are interesting additional experiments, but outside the scope of what we can manage. We have previously shown colocalization of Staufen, FMRP and UPF1 to these puncta (Graber et al, 2013; Graber et al, 2017) and shown that these puromycylated puncta also colocalize with nascent peptides detected using the Sun-Tag technique. While we think doing the experiment in the presence of an elongation inhibitor would be interesting, we disagree that it would prevent the reduction in WT puncta density, since we believe what is happening is the loss of the liquid-liquid phase separation of the ribosome clusters due to dephosphorylation of RBPs like FMRP and UPF1 (Graber et al, 2017), and this would reduce the puncta density whether or not the ribosomes were activated for translation.

Nevertheless, we have tried to temper the conclusions made from this result, emphasizing what we know (RPM puncta are decreased) as opposed to actual reactivation of stalled polysomes which we are not measuring.

> *Discussion - Page 18 - "Nevertheless, if FMRP binding was the critical determinant for presence in neuronal RNA granules, we would have expected to observe more differences." This is not true. If the data is poorly collected, you will not see differences.*

This statement was removed.

> *(16) "A proportion of the stalled ribosomes that are not stored in large RNA granules may still be pelleted in the sucrose gradients. This fraction may be greater in the absence of FMRP."*
>
> *Comment: The authors are right about this and touch on my original point that the characterization of the biochemical fractionation is not convincing enough. I'd suggest probing against more proteins that are contained in RNA granules.*

We have added several proteins to the biochemical characterization shown in Figure 1. We have added a discussion about the relationship between neuronal RNA granules and the sedimented pellet fraction in the discussion section.

https://doi.org/10.7554/eLife.106692.2.sa0